Sky coverage assessment for the European ELT: a joint evaluation for MAORY/MICADO and HARMONI

Cédric Plantet[a,†], **Benoît Neichel**[b,†], **Guido Agapito**[a], **Lorenzo Busoni**[a], **Carlos M. Correia**[c], **Thierry Fusco**[b,d], **Marco Bonaglia**[a], **Simone Esposito**[a]

[a]INAF, Osservatorio Astrofisico di Arcetri, Largo Enrico Fermi 5, 50125 Firenze, Italy
[b]Aix Marseille Univ, CNRS, CNES, LAM, Marseille, France
[c]Space ODT - Optical Deblurring Technologies, Rua Direita de Francos, 1021, R/C Esq 4250-194 Porto, Portugal
[d]ONERA, 29 avenue de la Division Leclerc, 92322 Chatillon, France

Abstract. The instruments developed for the upcoming Extremely Large Telescopes (ELTs) will need efficient Adaptive Optics (AO) systems to correct the effects of the atmospheric turbulence and allow imaging at the highest angular resolution. One of the most important requirement for ELT AO-assisted instruments will be to deliver diffraction-limited images in a significant part of the sky. For that, the instruments will be equipped with Laser Guide Stars (LGSs) providing most of the information required by AO instruments. But even with LGSs, AO systems still require the use of Natural Guide Stars (NGSs) to compensate for image motion (jitter) and some low order aberrations. These NGSs are eventually limiting the fraction of the sky that can be achieved by AO systems, the so-called Sky Coverage. In this paper, we first present the sky coverage assessment methods used for HARMONI (High Angular Resolution Monolithic Optical and Near-infrared Integral field spectrograph) and MAORY/MICADO (Multi-conjugate Adaptive Optics RelaY/Multi-AO Imaging Camera for Deep Observations), that are both instruments for the Extremely Large Telescope of the European Southern Observatory (ESO). They are based on a semi-analytical description of the main contributors in the AO error budget, allowing for a fast estimation of the residual jitter. As such, these methods are well suited for statistical estimation of the sky coverage on multiple science fields, and/or to efficiently explore the system parameter space. We then compute the sky coverage of the two instruments in cosmological fields from the Cosmic Assembly Near-IR Deep Extragalactic Legacy Survey (CANDELS) catalog. The goal is to provide an insight on the possibilities given by two different types of tomographic AO systems, i. e. Laser Tomography AO (LTAO) with HARMONI and Multi-Conjugate AO (MCAO) with MAORY, on the same telescope. In particular, we show that HARMONI and MAORY/MICADO are complementary, meaning that the overall sky coverage of ESO's ELT is much improved for applications common to both systems.

Keywords: Adaptive optics, Wavefront sensing, Multi-Conjugate Adaptive Optics, Laser Tomography Adaptive Optics, Extremely Large Telescope.

† co-first authors. Send all correspondence to cedric.plantet@inaf.it.

1 INTRODUCTION

The Extremely Large Telescope of the European Southern Observatory (ESO's ELT[1]) will have a theoretical resolution better than 15 milli-arcsec (mas) in K band, which will lead to observations of unprecedented quality. However, in order to reach this resolution in real conditions, it is necessary to compensate for the atmospheric turbulence effects on the incoming light with the help of an Adaptive Optics (AO) system. The AO system should be able to provide a satisfying performance

in a significant portion of the sky, i.e. a good Sky Coverage (SC), to allow the observation of many objects and consequently studies that are statistically robust.

The three first-light instruments of ESO's ELT, i. e. MAORY/MICADO (Multi-conjugate Adaptive Optics RelaY/Multi-AO Imaging Camera for Deep Observations),[2,3] HARMONI (High Angular Resolution Monolithic Optical and Near-infrared Integral field spectrograph)[4,5] and METIS (Mid-infrared ELT Imager and Spectrograph),[6] will first implement Single-Conjugated AO (SCAO) corrections. In this case, the AO system is using a single Natural Guide Star (NGS) and provides correction over a limited Field Of View (FoV) and SC. Indeed, this latter is limited by the fact that the SCAO system will typically require an NGS with a magnitude of R$<$14 within 10 arcsec.[7–9] The associated SC (or the probability to find such a configuration) is then only about 1% of the whole sky.[10] To improve the SC, the ELTs will implement multi-Laser Guide Stars (LGSs), providing bright artificial sources at any place over the sky.[11] The use of multi-LGSs can then significantly improve the SC. But LGSs suffer from two major limitations, known as cone effect and Tip-Tilt (TT) indetermination[12] . The first one (cone effect) is simply due to the fact that the LGS is produced at a finite distance (the Sodium layer at about 90km above the telescope), hence the volume of turbulence its light crosses is conic, whereas it would be cylindrical for a Natural Guide Star (NGS). This cone effect prevents the use of a single LGS for an ELT-size telescope and multiple LGSs (typically 6 to 8) are thus deployed, in order to pave the turbulent volume. This paving of the turbulence allows a tomographic reconstruction and the turbulent wavefront can then be corrected along the optical axis (Laser Tomography AO, or LTAO),[5] with a single Deformable Mirror (DM) as in SCAO, or even on a wider FoV (Multi-Conjugate AO, or MCAO), with several DMs optically conjugated to different altitudes.[13,14] The second main limitation (TT indetermination) comes from the fact that the laser light passes through the exact same path on the way up and

down.[15] Hence, the relative position of the LGS with respect to the background NGSs is unknown. As a first order, this means that the image position, or image jitter, cannot be compensated with a LGS. Therefore, all AO-LGS systems have to be complemented by the use of at least one NGS to control the fast image jitter induced by the atmospheric turbulence and other modes if needed. This or these NGSs can be faint, as only a few low order modes are to be evaluated, with typical foreseen limiting magnitude around H=19 for ESO's ELT.[5] They may also be chosen in a technical field of a few arcminutes, resulting in a typical SC better than 50%.

At this point it is important to properly define the notion of sky coverage. Indeed, to be meaningful, the SC has to be associated to a given performance.[16] This performance may be expressed in terms of residual jitter (e.g. in mas), in nanometers of wavefront error or in resulting Strehl Ratio, and the SC will be the fraction of the sky over which the AO system will be able to deliver this performance or better. It also important to emphasize that this performance will not be uniform across the sky, but will follow the density distribution of the stars. To a first order, SC will be 2 orders of magnitude better nearby the galactic plane than at the galactic poles, where the star density becomes very small.[17] Another illustrative example concerns the cosmological fields, where a large fraction of extra-galactic observations are done. In that sense, extra-galactic studies are not homogeneously distributed across the sky, but mostly concentrated on a few specific fields, where multi-wavelengths observations are available. Those fields have generally been chosen to be located outside of the galactic plane in order to avoid contamination by dust, but also, in regions lacking bright stars to allow for long expositions without risk of science detectors saturation.[18] This is obviously perpendicular to the AO needs in terms of NGS requirements, and biases the SC. But as these fields are of particular interest for the astronomical community, it is of importance to estimate the AO performance in these specific regions.

In this paper, we focus on the SC estimation of the two tomographic AO systems respectively providing a correction for HARMONI and MICADO. The first one is a LTAO system, called H-LTAO, and the second one, MAORY, is an MCAO system. We first present the sky coverage assessment methods of the two instruments. These methods are very similar and are based on an analytical description of the jitter control, which allows for a fast estimation of the performance. This latter point is crucial in the design phases of instrument, as one wants to explore a wide system and atmospheric parameter space. This also allows for statistical studies of SC, computing the performance for hundreds of scientific fields. Taking advantage of this computational capability, we compute the SC of H-LTAO and MAORY in synthetic fields from the Besancon galaxy model[19] and in known cosmological fields from the Cosmic Assembly Near-IR Deep Extragalactic Legacy Survey (CANDELS) catalog.[20,21] This comparison gives an insight on the possibilities provided by each instrument. In particular, we show that they have a complementary SC, meaning that the overall sky coverage is greatly improved for applications that are common to both systems.

The assumptions and simulation inputs are presented in Section 2, the semi-analytical methods are presented in Section 3 and the applications on synthetic fields and on cosmological fields are presented in Section 4. Finally, we discuss the results and conclude in sections 5 and 6.

2 Assumptions and tools

In this section, we list the tools and the default assumptions used throughout the study.

2.1 Error budget approach

In order to assess the performance in a given configuration, one needs either to perform a full end-to-end (E2E) simulation and/or use analytical/semi-analytical tools. In this latter approach, the

fundamental assumption is that all the contributors to the final performance are fully uncorrelated and can be estimated independently. This is an error budget approach, where the final performance is the result (the sum) of independent contributors. This approach is convenient as typically each term of the error budget can be estimated by analytical formulae, which makes the whole process extremely fast when compared to full E2E simulations. Of course, the performance assessment will not be as accurate as with E2E simulations, but it allows to narrow the parameter space efficiently. In this study we will follow this error budget approach, with the first assumption that all the High-Order (HO) part of the error budget (related to the LGSs measurements) are evaluated independently. We thus only focus on the Low-Order (LO) part of the error budget, and mostly on the residual jitter estimation.

2.2 Atmospheric parameters

The studies for both systems have been done using the same C_n^2 profiles, that were provided by ESO.[22] Most of the SC study relies on the median profile, that has 35 layers ranging from 30 m to 26500 m, with 70% of the turbulence below 600 m (approximate conjugation altitude of M4, the DM of ESO's ELT). The median seeing is 0.644" (defined at zenith and at 500 nm) and the outer scale is 25 m. The other C_n^2 profiles correspond to the 4 quartiles. They are very similar to the median profile in terms of energy distribution, but they have different seeings. In the following, we also assume that all the performances are estimated for a zenith angle of 30°.

2.3 System parameters

Being both tomographic AO systems, MAORY and H-LTAO have some similarities. However, they still are two different types of system, with different requirements: H-LTAO should provide a

good correction only on axis, while MAORY should provide a wide-field correction. Another main difference is the patrol field of the NGS wavefront sensors, a.k.a. technical FoV: H-LTAO can pick its NGS close to the axis, while MAORY must make use of NGSs far off axis to avoid vignetting the scientific FoV. However, MAORY's NGSs can get a bit closer to the axis when MICADO uses its small FoV, as the vignetting area decreases. The configuration for each system is listed in Tab. 1. The optimized FoV as stated in the table is the so-called FoV of interest in Fusco et al.[23]

Table 1: System configurations for H-LTAO and MAORY. For MAORY, the DM configuration is presented as baseline / upgrade. The inner border radius of MAORY's technical FoV takes into account the potential vignetting of the scientific FoV by the pick-off mirrors. The LGSs are uniformly distributed on a circle of the specified radius.

Parameter	MAORY	H-LTAO
Technical FoV (radius)	annulus: 49" - 80" (24" - 80" for small MICADO FoV)	60"
# DMs	baseline: 2 upgrade: 3	1
DM altitudes	baseline: 621 m (M4), 17.6 km upgrade: 621 m (M4), 7.4 km, 17.6 km	621 m (M4)
DM pitches	baseline: 0.5 m, 1.5 m (970 modes) upgrade: 0.5 m, 1 m (1690 modes), 1.5 m (970 modes)	0.5 m
# LGSs	6	6
# NGSs	up to 3	1
LGS asterism radius	45"	34"
# modes on the NGSs	2 (Tip/tilt)	2 (Tip/tilt)
# subapertures (NGS sensors)	2×2	2×2
Optimized FoV radius	30"	0" (on axis only)

The NGS wavefront sensors (WFS) for both MAORY and H-LTAO will have 2×2 subapertures to be able to sense the focus at lower frequency and correct the sodium layer altitude variations on the LGS WFSs.[24] In the following, we consider these sensors as tip/tilt sensors only (with the appropriate noise due to their subaperture geometry) and we add a fixed amount of focus in the error budget, that is the residual of the sodium altitude variations.

For H-LTAO, given that the Strehl Ratio (SR) on the NGSs might be low because of the off-axis distance, a solution to increase the signal-to-noise ratio on the NGS WFSs has been considered in the SC study. This solution consists in adding an Open-Loop DM (OLDM) in the path of the NGS WFS. This so-called Dual AO[25] would correct up to a few hundred wavefront modes in order to increase the sensitivity of the NGS WFSs. This solution is not required for MAORY, as the multiple DMs in the path can compensate for the atmosphere in a wider FoV.

2.4 Windshake

The secondary mirror (M2) of ESO's ELT will be close to the dome aperture and thus undergo a rather strong wind in some cases, causing high-amplitude vibrations. ESO provided the first-light instruments consortia with a data package,[26] in which one can find a 300 seconds time series of the wavefront tip/tilt due to such a windshake. This time series corresponds to a worst case scenario: external wind 10 m/s (scenario), wind in the dome 8 m/s (scenario), frontal wind w.r.t. the telescope (worst condition), telescope zenith distance pointing 45° (worst condition for frontal wind), wind screen deployed up not to vignette the telescope aperture (normal operating setup). The temporal Power Spectral Densities (PSD) of the tip and tilt corresponding to the time series are plotted in Fig. 1. Depending on the telescope orientation with respect to the wind direction, one axis can be more excited than the other, which is the case in this scenario where the tilt gathers more energy than the tip. The tip/tilt from the windshake is isoplanatic (according to ESO studies), so one NGS is sufficient to sense it.

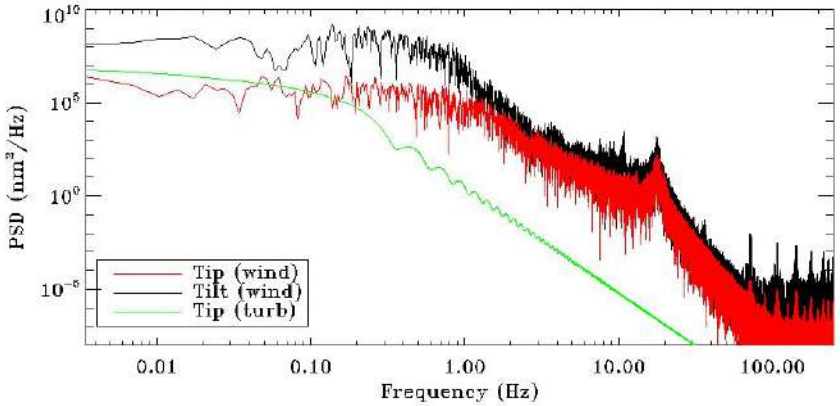

Figure 1: Temporal PSDs of the tip/tilt due to the windshake on M2, compared to the turbulence PSD. The PSDs are computed from the time series using a Hanning window.

Several strategies can be adopted for the correction:

- Telescope only: The windshake is corrected using the telescope probes only. The residual jitter is then independent from the NGS asterism used by the AO system.
- Sequential: The windshake is only corrected by one of the NGS sensors of the AO system.
- Cascaded: The windshake is mostly corrected by the telescope, then the residual is corrected by the NGS sensors of the AO system.

For H-LTAO, the 2 last approaches are considered, while only the sequential control has been studied for MAORY.

2.5 Stars statistics

The sky coverage analysis requires a list of stars with their respective positions and magnitudes. This list can either be directly taken from a real star catalog or generated from a galaxy model. In the latter case, stars are randomly placed with a uniform distribution in the FoV corresponding to the query. In the following we show results both with the CANDELS catalog[20,21] and with the Besancon galaxy model.[19]

3 Sky coverage assessment method

The approaches of MAORY and H-LTAO to assess the SC are very similar, as they follow the same steps. We describe these steps hereafter, specifying the differences between the two systems.

3.1 Asterism selection

At this point we have a list of star positions and magnitudes in a wide FoV, and we generate a series of pointing coordinates with a uniform distribution. For each pointing, in the case of MAORY, we register all asterisms that are geometrically valid with respect to the technical FoV size, the pick-off mirror size and the overlap between sensors (Fig. 2). If no 3-star asterism is found, we look for 2-star asterisms. Again, if we find no valid asterism, we select each star individually. The reason why we do not consider all asterisms (1 NGS, 2 NGSs or 3 NGSs) is purely computational. In the case of H-LTAO, we use only one NGS and there are no zonal constraints, we thus compute the performance for each individual NGS within the technical FoV.

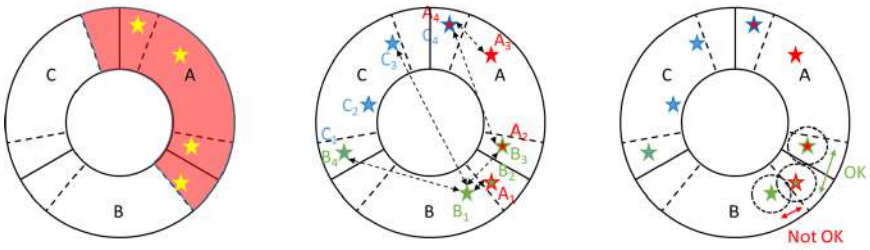

Figure 2: Method to detect a valid configuration in the case of MAORY. The sensors' dedicated working areas are delimited by the solid lines, while the dashed lines indicate the possible extension of these areas. Between two dashed lines, we thus have an overlap zone between two sensors. Steps are, from left to right: 1) Register all the stars under the limiting magnitude reachable by each sensor (remove those too close to the center to avoid vignetting). In this figure we show the example for WFS A (the same is done for WFSs B and C). The red color shows the total area eventually reachable by the WFS A. Here the star symbols are the potential NGSs for this sensor. 2) Compute distances between the registered stars. Here the stars are color-coded as a function of which sensor can reach it (filling color = dedicated zone, contour color = overlap zone): red for WFS A, green for WFS B and blue for WFS C. They are also named accordingly as indicated in the figure (a star reachable by two sensors will have two names). 3) Check the combinations that avoid collisions of the pick-off mirrors. For example, B2/A1 cannot be selected together with B1, but it can be selected together with B3.

3.2 Performance computation

The final performance is computed from these different terms:

- High orders: Residuals from the LGS sensing.
- Low orders: Residuals from the NGS sensing.
- Additional error: Constant residual from various sources (non AO-correctable). This includes, but is not limited to, wavefront errors due to non-common path aberrations, misalignment and manufacturing.

The LO residuals are themselves separated in 3 parts: windshake, anisoplanatism/tomography, noise propagation. We consider the temporal error from the low orders negligible with respect to the rest of the error budget.

3.2.1 *High orders*

For MAORY, the HO residuals are derived from E2E simulations, with an equilateral triangle of bright NGSs (H = 10) at 55". We verified that the HO residuals variation with the NGS asterism is negligible. We add a fixed amount of 190 nm, corresponding to non AO-correctable errors or other isoplanatic residuals, to these E2E residuals and we get the following HO residuals for the respective distances 0", 15", 25" and 30":

- M4 + 1 Post-Focal DM (PFDM): 302 nm, 304 nm, 313 nm and 324 nm.
- M4 + 2 PFDMs: 298 nm, 302 nm, 308 nm and 314 nm.

For H-LTAO, the HO residuals are also derived from E2E simulations, including all the atmospheric and telescope effects, but using a bright on-axis NGS. The performance is only to be estimated on-axis, and provides an error budget of 270 nm.

3.2.2 *Windshake*

As stated in section 2.4, 2 different strategies can be considered: sequential or cascaded.

For the sequential control, the windshake is sensed on the brightest available NGS. Indeed, with the AO system alone, a high loop frequency is needed to be able to correct the high-amplitude tip-tilt induced by the windshake. The residual tip/tilt is then computed by applying a temporal filter to the windshake PSD. This filter is:

- H-LTAO: a Linear Quadratic Gaussian (LQG) + second-order Auto Regressive (AR2) command. The filter is optimized for the control update based on the NGS magnitude.
- MAORY: a filter of order 2, with its poles, zeros and gain optimized with respect to the NGS magnitude and SR, i. e. with respect to the noise level.

The residual in Mean Square Error (MSE) is then:

$$\mathrm{MSE} = \int_0^\infty \left[|\mathrm{RTF}|^2 \, \mathrm{PSD}_{\mathrm{wind}} + |\mathrm{NTF}|^2 \, \mathrm{PSD}_{\mathrm{noise}} \right] df \tag{1}$$

with RTF the Rejection Transfer Function and NTF the Noise Transfer Function corresponding to the temporal filter. The computation of the noise level for H-LTAO is described in section 3.2.4. For MAORY, the noise level is computed from a Gaussian Point Spread Function (PSF) model, with the flux scaled with the SR, and from the weighting maps used for local slope computation. Note that this method, that should lead to results similar to the ones of H-LTAO, is only used for the windshake residual computation, and the noise considered for the tomographic correction of atmospheric tip/tilt is the one described in section 3.2.4.

The cascaded mode (only considered for H-LTAO) is a mix of the telescope and instrument control. The windshake PSD becomes a residual tip/tilt PSD, but an arbitrary level of jitter is still added to account for the errors related to the telescope probes. In this case, the command is optimized in frequency according to the noise level, hence according to the NGS magnitude and SR.

3.2.3 Pure tomographic error

The pure tomographic error is due to the asterism geometry. For MAORY, it is computed using the method detailed in Appendix A. For H-LTAO, only one NGS is used, so the tomographic error simply is the anisoplanatism error, that can be retrieved from the same formulas.

3.2.4 Noise propagation

For MAORY, in order to have a measurement noise level as a function of a star's distance and magnitude, we perform a series of E2E simulations changing only the NGS asterism, and we repeat it for 5 atmosphere occurrences. The NGSs are always on an equilateral triangle and all have the same magnitude. The loop frequency is adapted to the magnitude. In the end, we have a total of 5×18 simulations for each considered configuration, using the following distances and magnitudes:

- Distance: 30", 55", 65" and 80".
- H magnitude: 10, 17, 18, 19, 20, 21.

For each of these simulations, the residual in the directions of the NGSs is averaged, so that we have a residual per distance and magnitude. Then, for each star of each asterism considered in the SC computation, we interpolate these residuals at the star's distance and magnitude and consider the obtained value as the noise level on that star. This means that we also include the aliasing error and the temporal error in the noise term. It does not have a significant impact on the final residual, since the aliasing error propagates the same way as the noise in the loop and we can consider the temporal error to be negligible with respect to the other terms (it amounts to about 0.4 mas at the faint end). The noise term is then propagated through the tomographic reconstructor as described in Appendix A. Note that this computation remains the same for both MICADO's large and small FoVs. The only difference between the two configurations is in the asterism selection.

In the case of H-LTAO, the noise on the Shack-Hartmann (SH) slopes has been computed based on E2E simulations, from which general abacuses are derived. The basic scheme of the E2E simulation is described by Fig. 3, and follows 5 steps: (1) Computation of short exposure SH PSFs

for various LTAO configurations and for various positions in the FoV. This computation includes the full telescope pupil parameters (central obstruction value for instance) and Shark-Hartmann configurations (number of sub-aperture, wavelength), (2) Known tilts are then added to each PSF, (3) Additional defects (Atmospheric Dispersion Corrector residuals, static aberrations, object size) can also be added, as well as various types of noise (photon, background, read-out-noise), (4) centroiding is measured on those Shack-Hartmann images, with several possible techniques, (5) the Tilt is reconstructed from the measurement, leading to the residual Tilt error and variance.

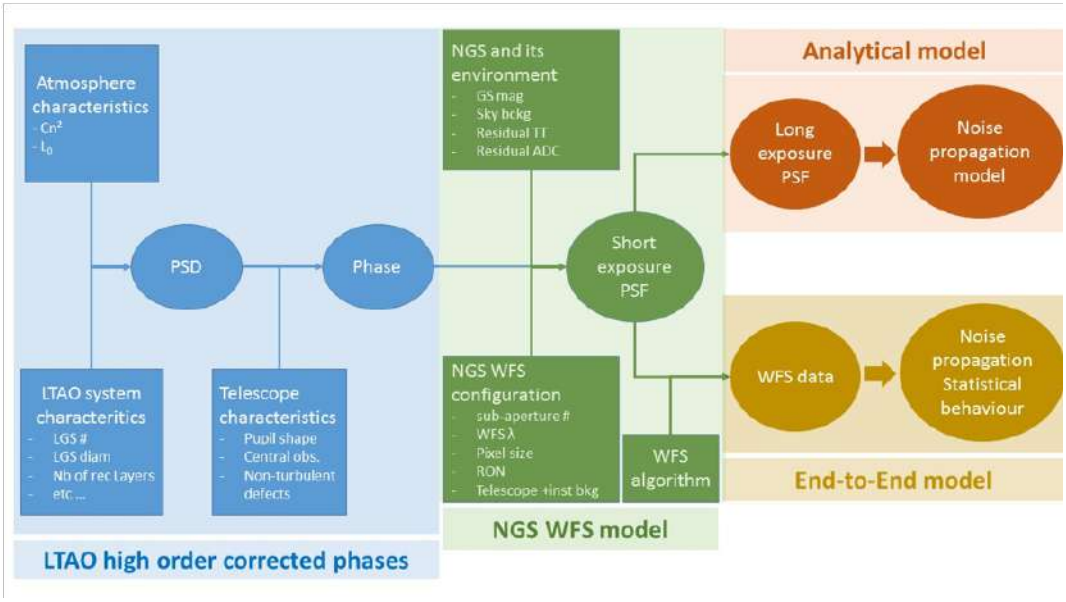

Figure 3: Global scheme of the E2E TT noise estimation.

This procedure is repeated for different position in the field, hence different level of AO correction. As an illustration, Fig. 4 shows the one axis Tilt error variance for different number of photons and different positions of the NGS in the field. As a reference, 200 photons per frame correspond to a magnitude H=18.5. This plots are then fitted with analytical formulas (see next equations), which will eventually be used in the sky coverage analysis.

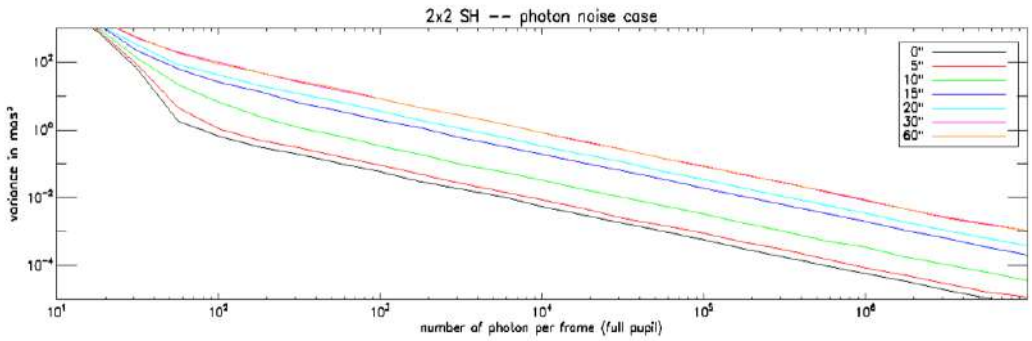

Figure 4: Example of noise computed for a 2x2 SHWFS, for different level of fluxes, and different position of the NGS in the field, in the case of an LTAO correction without OLDM.

In order to account for the residual phase (and thus the spread of photons outside the diffraction core), the analytical variance formulas (as defined in Nicolle *et al.*[27]) have to be modified as follows, for the photon noise and the Read-Out Noise (RON):

$$\sigma^2_{ph,sspup,SR} = \frac{1}{SR\ 2\ ln(2) N_{ph}} \frac{N_T^2}{N_D^2} \left(\frac{N_T^2 + N_W^2}{2N_T^2 + N_W^2} \right)^2 \tag{2}$$

$$\sigma^2_{ron,sspup,SR} = \frac{\pi}{SR^2\ 32\ ln(2)} \frac{ron^2}{N_{ph}^2} \left(\frac{N_T^2 + N_W^2}{N_D^2} \right)^2 \tag{3}$$

where N_{ph} is the number of photons, N_D is the Full Width at Half Maximum (FWHM) of the diffraction-limited PSF, N_T is the FWHM of the actual PSF, and N_W the FWHM of the weighting function used for the Weighted Center of Gravity.

When the PSF is no more diffraction limited, the FWHM (N_T) becomes the major contributor of the variance and the noise variances become again the classical ones:

$$\sigma^2_{ph,sspup,FWHM} = \frac{1}{2\ ln(2) N_{ph}} \frac{N_T^2}{N_D^2} \left(\frac{N_T^2 + N_W^2}{2N_T^2 + N_W^2} \right)^2 \tag{4}$$

$$\sigma^2_{ron,sspup,FWHM} = \frac{\pi}{32\ ln(2)} \frac{ron^2}{N^2_{ph}} \left(\frac{N^2_T + N^2_W}{N^2_D} \right)^2 \quad (5)$$

In practice, we will use a combination of both analytic expressions in order to account for both regimes. This is done using the following ad-hoc expression:

$$\sigma^2_{tot} = \left(\frac{N_D}{N_T} \right)^2 \sigma^2_{SR} + \left(1 - \left(\frac{N_D}{N_T} \right)^2 \right) \sigma^2_{FWHM} \quad (6)$$

In the SC study described below, the analytical laws will be used, which will allow us to quickly estimate the measurement noise for different NGS magnitude and position in FoV, as well for different configurations (central wavelength, number of subapertures, RON, elongation due to Atmospheric Dispersion Corrector residual etc...).

A numerical validation of the noise models presented in this section is shown in Appendix C.

3.3 Sky coverage computation

At this point, we are able to compute the jitter/SR for any direction in the scientific FoV, and thus compute the SC.

For each pointing, we compute the LO residuals in the scientific FoV with all the possible asterisms and we register the lowest residual. For H-LTAO, we only need to compute the residual on axis, while for MAORY, the selection of the best asterism is based on the average LO residual in the FoV (using the directions shown in Fig. 5). We then add the HO residuals given in section 3.2.1 to calculate the SR. Finally, we get the SC as the ratio between the number of fields giving a

SR (jitter) greater (less) or equal to a given value and the total number of fields:

$$SC(x) = \frac{\sum_i P_i(SR \geqslant x)}{N_{fields}} \quad \text{or} \quad SC(x) = \frac{\sum_i P_i(jitter \leqslant x)}{N_{fields}} \tag{7}$$

with $P_i(SR \geqslant x) = 1$ ($P_i(jitter \leqslant x) = 1$) if the i-th field has an asterism giving a SR (jitter) greater (less) than x and $P_i(SR \geqslant x) = 0$ ($P_i(jitter \leqslant x) = 0$) otherwise.

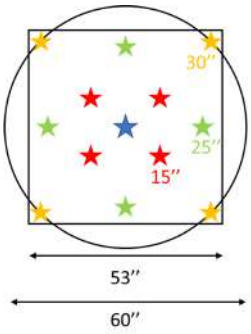

Figure 5: Directions used for the jitter/SR computation in the FoV of diameter 60". The square of side 53" corresponds to the large MICADO FoV. The stars are distributed as follows: 1 star on axis, 4 stars at 15", 4 stars at 25" and 4 stars at 30". When the small MICADO FoV is considered (20×20"), we average from 1 star on axis and 4 stars at 10" (placed in the same manner as the 4 stars at 15").

4 Sky coverage examples

4.1 Synthetic star fields

We first show an example of sky coverage computation with the Besancon galaxy model for two regions of the sky: 1×1 degrees at the following galactic coordinates: $l = 90°, b = -30°$ and $l = 90°, b = -60°$. The results are plotted in Figs. 6 and 7 and the main numbers are reported in Tabs. 2 and 3. Here we see the effect of the star density decreasing when going further from the galactic plane: lower jitter, or higher SR, can be obtained in all cases at $b = -30°$ with respect to $b = -60°$.

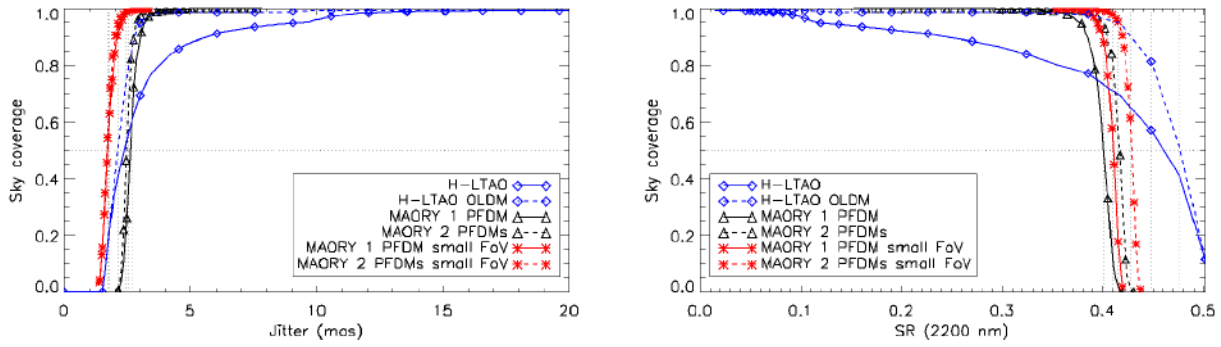

(a) Jitter (b) SR

Figure 6: Sky coverage with H-LTAO or with MAORY at $l = 90°, b = -30°$. The jitter/SR is on axis for H-LTAO and averaged on a 1 arcmin diameter FoV (Large FoV) or on a 20" diameter FoV (small FoV) for MAORY.

Instrument/configuration	Jitter (mas)			SR (2200 nm)		
	25% SC	50% SC	75% SC	25% SC	50% SC	75% SC
H-LTAO	2	2.4	3.3	0.48	0.45	0.38
H-LTAO OLDM	1.8	2.1	2.6	0.48	0.48	0.45
MAORY 1 PFDM	2.4	2.6	2.8	0.41	0.4	0.39
MAORY 2 PFDMs	2.4	2.5	2.6	0.42	0.41	0.41
MAORY 1 PFDM small FoV	1.6	1.8	2	0.45	0.45	0.44
MAORY 2 PFDMs small FoV	1.6	1.7	1.9	0.46	0.45	0.45

Table 2: Jitter/SR reached by the considered systems for different levels of sky coverage at $l = 90°, b = -30°$.

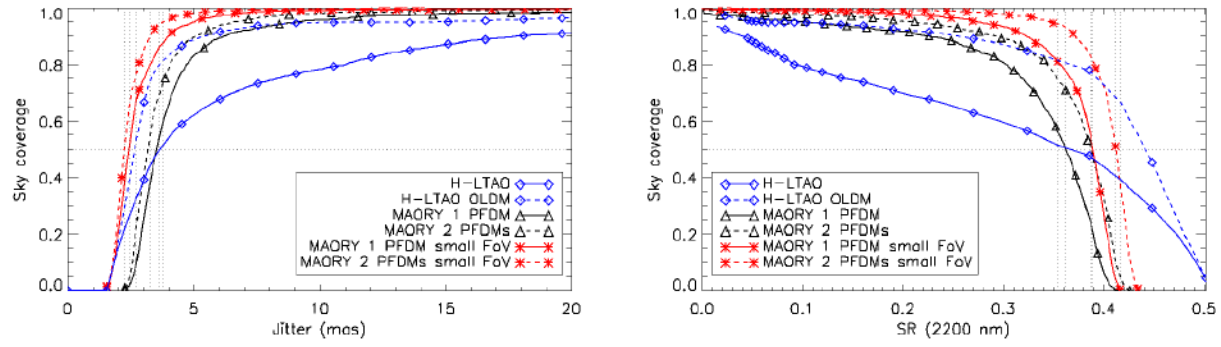

(a) Jitter (b) SR

Figure 7: Sky coverage with H-LTAO or with MAORY at $l = 90°, b = -60°$. The jitter/SR is on axis for H-LTAO and averaged on a 1 arcmin diameter FoV (Large FoV) or on a 20" diameter FoV (small FoV) for MAORY.

Instrument/configuration	Jitter (mas)			SR (2200 nm)		
	25% SC	50% SC	75% SC	25% SC	50% SC	75% SC
H-LTAO	2.4	3.8	8.3	0.45	0.35	0.14
H-LTAO OLDM	2.3	2.7	3.3	0.45	0.42	0.38
MAORY 1 PFDM	3	3.6	4.4	0.38	0.36	0.32
MAORY 2 PFDMs	2.8	3.3	3.9	0.4	0.39	0.35
MAORY 1 PFDM small FoV	2.1	2.4	3	0.43	0.42	0.4
MAORY 2 PFDMs small FoV	2	2.2	2.7	0.44	0.44	0.42

Table 3: Jitter/SR reached by the considered systems for different levels of sky coverage at $l = 90^\circ, b = -60^\circ$.

4.2 Application for real cosmological fields

We now apply the SC computation to cosmological fields that are taken from the CANDELS catalogs.[20] The five specific fields are shown in Fig. 8, with namely COSMOS, UDS, EGS, GOODS-S and GOODS-N[1]. Table 4 summarizes some of the important characteristics of these fields for our present study.

Field Name	RA	DEC	Area	# of stars with H(Vega)<21
GOODS-S	03h32m30s	-27°48'20"	$\sim$160arcmin^2	620
GOODS-N	12h36m55s	+62°14'15"	$\sim$160arcmin^2	240
UDS	02h17m49s	-05°12'02"	$\sim$204arcmin^2	321
COSMOS	10h00m28s	+02°12'21"	$\sim$204arcmin^2	474
EGS	14h17m00s	+52°30'00"	$\sim$205arcmin^2	348

Table 4: Location, area and depth of the 5 cosmological fields used in the sky coverage estimation for MAORY and HARMONI.

These fields have been observed deeply and at multiple wavelengths with the Hubble Space Telescope as well as many other instruments. As such, they are privileged fields for extra-galactic studies, and will likely be observed extensively with ESO's ELT. However, the fields considered here correspond to regions where bright NGSs are few, as they were chosen to facilitate the imaging of extra-galactic objects. Of course, this is at the opposite of what the AO system requires to give an

[1]Note that GOODS-N and EGS will not be observable from ESO's ELT location. We still keep it for the sky coverage analysis as it provides a representative example of cosmological fields.

optimal performance. Therefore, evaluating the performance of the AO-assisted ELT instruments on these specific fields is or particular importance. These fields are also of interest as the catalogs available are complete down to H<26 (Vega), which is 5 magnitudes deeper than what is required by the AO systems. All the technical details about these fields can be found in Grogin et al.,[20] in the following we only made use of the publicly available H-band catalogs.

Figures 9, 10, 12, 13, 15, 16, 18, 19, 21 and 22 give the evaluated jitter and SR maps for these fields, and the statistics of the jitter and SR for each field are given in Figs. 11, 14, 17, 20 and 23. The main numbers of these statistics are reported in Tabs. 5 to 9. Note that we also consider the case in which the MICADO FoV is smaller (20×20"). In this configuration, the NGSs sensors of MAORY can reach stars closer to the axis, as shown in Tab. 1. The performance is then averaged as indicated in Fig. 5.

It is interesting to note that MAORY, with the large MICADO FoV, never reaches the minimum jitter (i. e. the jitter at 0% SC, see for example Fig. 11) as low as the one from H-LTAO: the best available asterism for MAORY is not the best that the system could actually expect with an infinite number of bright stars, while the best case for H-LTAO (i. e. an on-axis bright NGS) does happen here. The ability of AO systems to deal with this type of situation is particularly interesting as we are looking at the limits of their performance in presence of only few NGSs.

The two systems also offer a similar peak performance, with a SR of about 45% in K band [2] and a few mas of jitter. The median performance is quite dependent on the field and/or the configuration of the system: the median jitter is below 5 mas for the best fields (COSMOS and UDS), leading to median SRs ranging between 30 and 40%, while the median jitter in the worst field

[2]We recall that MAORY's performance is averaged on the whole scientific FoV, hence its peak performance on axis is higher (typically a few points of SR) than the numbers written here.

(GOODS-N) can go up to between 10 and 15 mas for the lowest-performing configurations, leading to median SRs below 10%. Better configurations (H-LTAO with the OLDM, MAORY with 2 PFDMs and/or with the small MICADO FoV) provide better robustness, with median SRs roughly ranging between 10 and 20% in the GOODS-N field. From this results, we can derive approximate equivalencies between the two systems. H-LTAO without the OLDM gives a performance that approximately is between MAORY's baseline configuration (1 PFDM, large MICADO FoV) and the upgraded configuration (2 PFDMs, large MICADO FoV), though it provides a better SC at both ends (low SC/high performance and high SC/low performance). With the OLDM in H-LTAO, the performance gets similar to what we can expect with the small MICADO FoV for MAORY. In that case, the performance is closer to MAORY with 2 PFDMs at both ends and to MAORY with 1 PFDM in the knee of the SC curve.

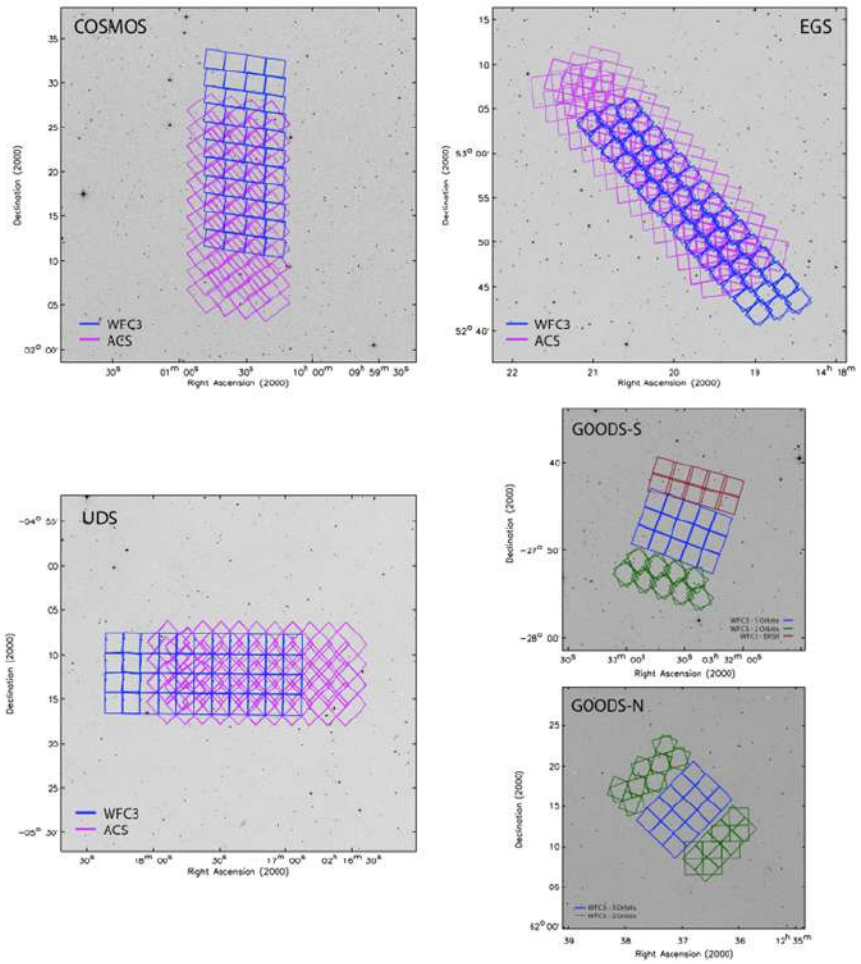

Figure 8: Cosmological fields considered in this section. Taken from Grogin et al.[20].

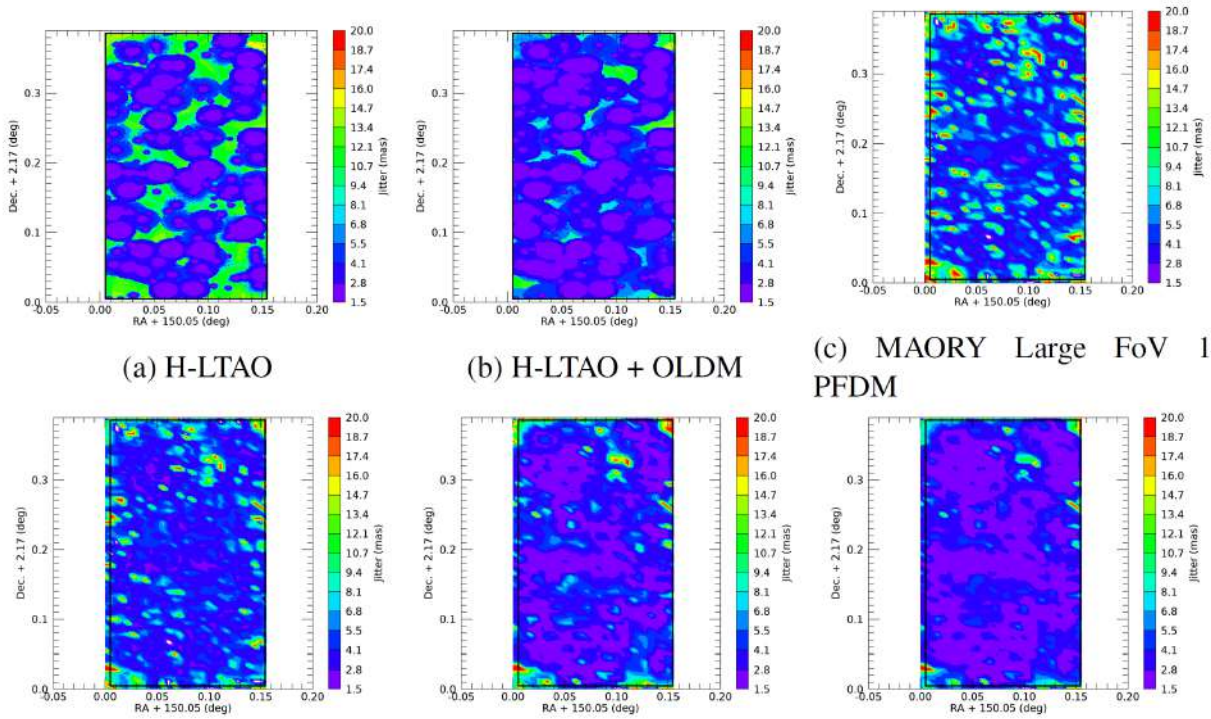

(a) H-LTAO (b) H-LTAO + OLDM (c) MAORY Large FoV 1 PFDM

(d) MAORY Large FoV 2 PFDMs (e) MAORY Small FoV 1 PFDM (f) MAORY Small FoV 2 PFDMs

Figure 9: Jitter with H-LTAO (on axis) or with MAORY (averaged on the scientific FoV) for the COSMOS field. The jitter is limited to 20 mas for a better display. The black lines indicate the area used for the sky coverage computation.

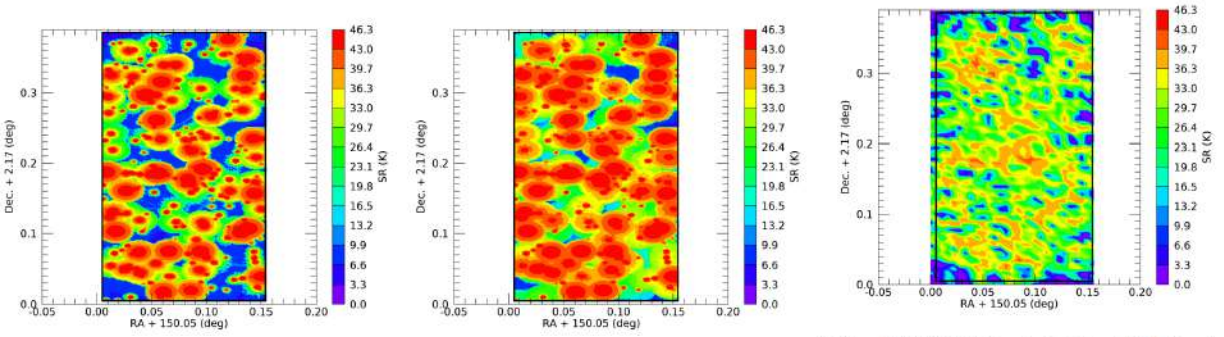

(a) H-LTAO (b) H-LTAO + OLDM (c) MAORY Large FoV 1 PFDM

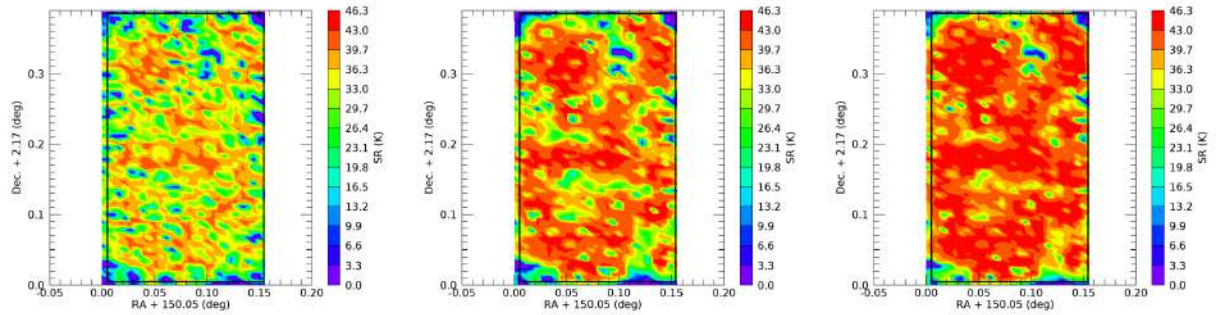

(d) MAORY Large FoV 2 PFDMs (e) MAORY Small FoV 1 PFDM (f) MAORY Small FoV 2 PFDMs

Figure 10: Strehl ratio in K band with H-LTAO (on axis) or with MAORY (averaged on the scientific FoV) for the COSMOS field. The black lines indicate the area used for the sky coverage computation.

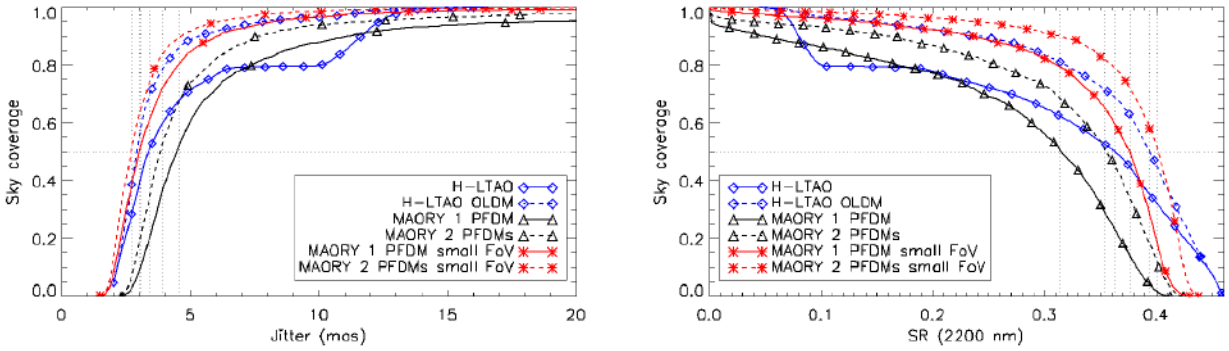

(a) Jitter (b) SR

Figure 11: Sky coverage with H-LTAO or with MAORY for the COSMOS field. The jitter/SR is on axis for H-LTAO and averaged on a 1 arcmin diameter FoV (Large FoV) or on a 20" diameter FoV (small FoV) for MAORY.

Instrument/configuration	Jitter (mas)			SR (2200 nm)		
	25% SC	50% SC	75% SC	25% SC	50% SC	75% SC
H-LTAO	2.6	3.4	5.7	0.41	0.36	0.22
H-LTAO OLDM	2.5	3	3.7	0.42	0.39	0.34
MAORY 1 PFDM	3.6	4.6	6.4	0.36	0.31	0.22
MAORY 2 PFDMs	3.2	3.9	5.2	0.39	0.35	0.29
MAORY 1 PFDM small FoV	2.4	3.1	4.2	0.42	0.4	0.34
MAORY 2 PFDMs small FoV	2.3	2.7	3.5	0.44	0.42	0.38

Table 5: Jitter/SR reached by the considered systems for different levels of sky coverage in the COSMOS field.

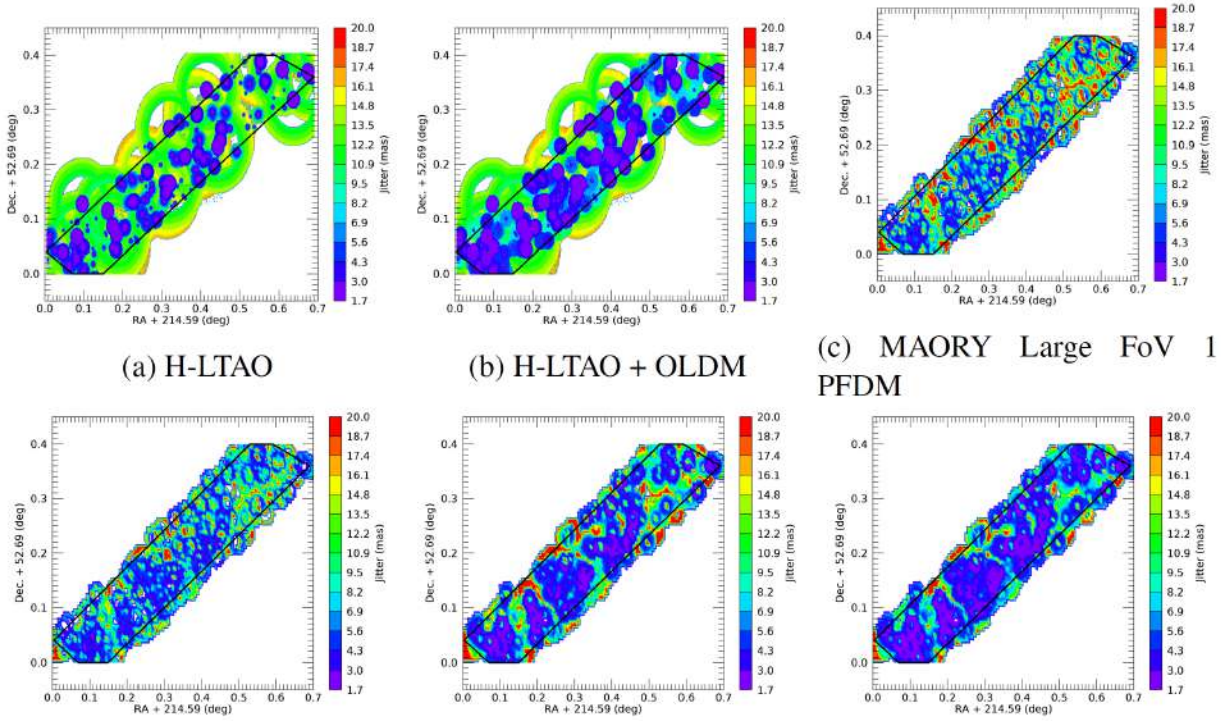

(a) H-LTAO (b) H-LTAO + OLDM (c) MAORY Large FoV 1 PFDM

(d) MAORY Large FoV 2 PFDMs (e) MAORY Small FoV 1 PFDM (f) MAORY Small FoV 2 PFDMs

Figure 12: Jitter with H-LTAO (on axis) or with MAORY (averaged on the scientific FoV) for the EGS field. The jitter is limited to 20 mas for a better display. The black lines indicate the area used for the sky coverage computation.

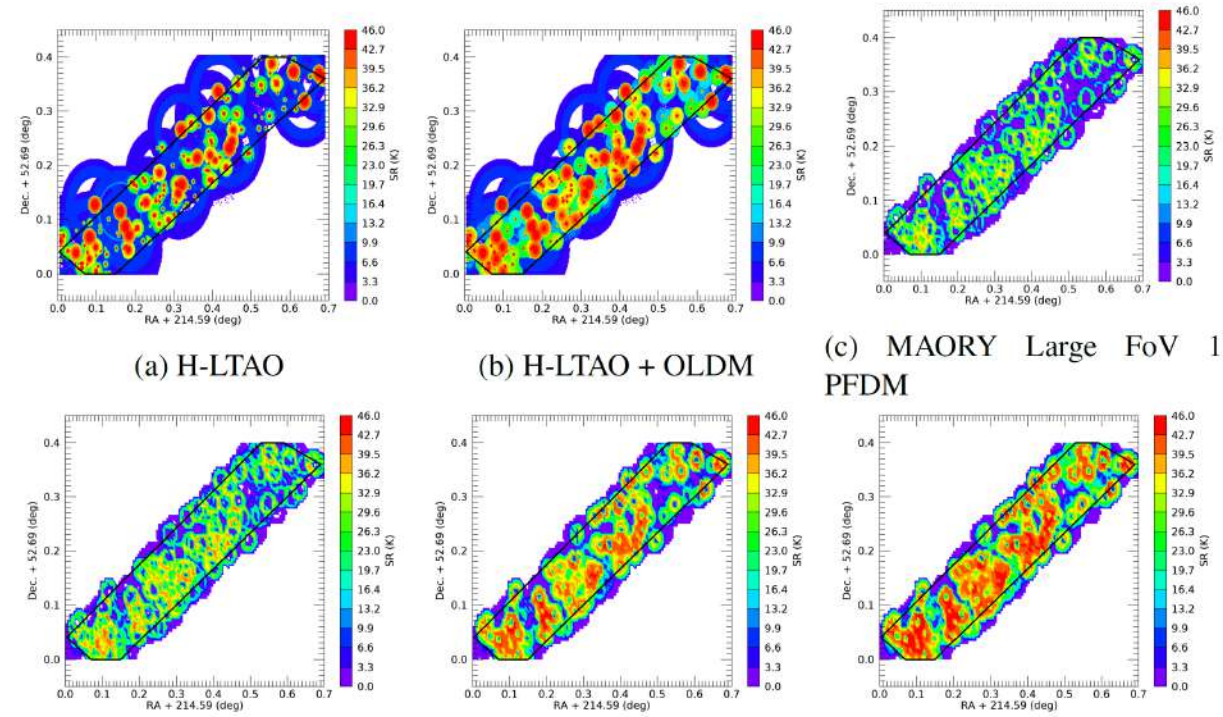

(a) H-LTAO (b) H-LTAO + OLDM (c) MAORY Large FoV 1 PFDM

(d) MAORY Large FoV 2 PFDMs (e) MAORY Small FoV 1 PFDM (f) MAORY Small FoV 2 PFDMs

Figure 13: Strehl ratio in K band with H-LTAO (on axis) or with MAORY (averaged on the scientific FoV) for the EGS field. The black lines indicate the area used for the sky coverage computation.

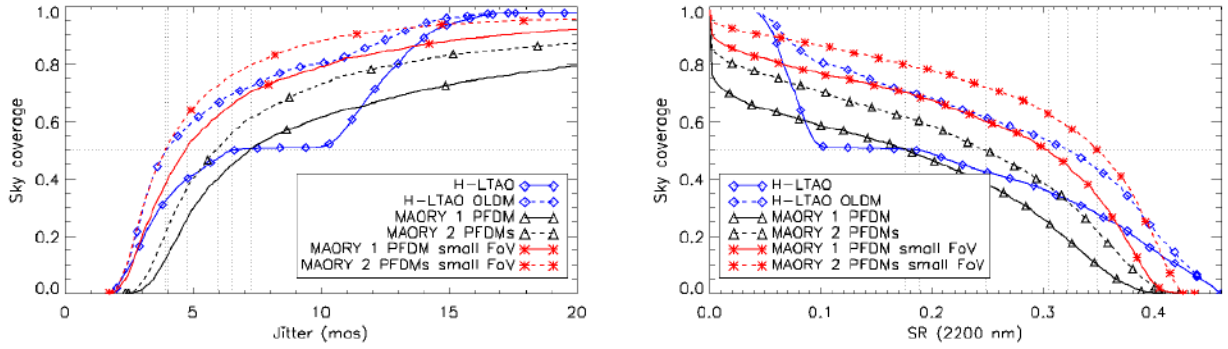

(a) Jitter (b) SR

Figure 14: Sky coverage with H-LTAO or with MAORY for the EGS field. The jitter/SR is on axis for H-LTAO and averaged on a 1 arcmin diameter FoV (Large FoV) or on a 20" diameter FoV (small FoV) for MAORY.

Instrument/configuration	Jitter (mas)			SR (2200 nm)		
	25% SC	50% SC	75% SC	25% SC	50% SC	75% SC
H-LTAO	3.4	6.5	12.5	0.36	0.19	0.07
H-LTAO OLDM	3	4	8	0.39	0.32	0.14
MAORY 1 PFDM	4.8	7.3	16.4	0.30	0.18	0
MAORY 2 PFDMs	4.2	6	10.6	0.34	0.25	0.06
MAORY 1 PFDM small FoV	3.2	4.7	8.6	0.39	0.31	0.12
MAORY 2 PFDMs small FoV	2.9	3.9	6.4	0.41	0.36	0.23

Table 6: Jitter/SR reached by the considered systems for different levels of sky coverage in the EGS field.

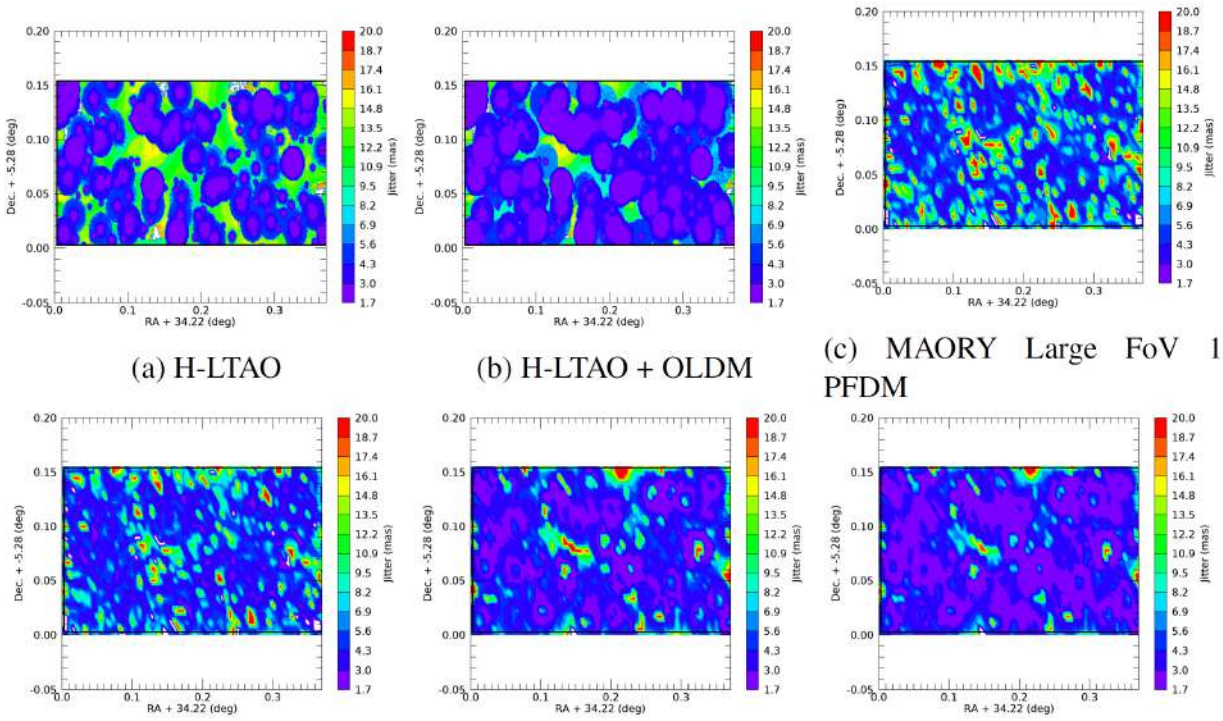

(a) H-LTAO (b) H-LTAO + OLDM (c) MAORY Large FoV 1 PFDM

(d) MAORY Large FoV 2 PFDMs (e) MAORY Small FoV 1 PFDM (f) MAORY Small FoV 2 PFDMs

Figure 15: Jitter with H-LTAO (on axis) or with MAORY (averaged on the scientific FoV) for the UDS field. The jitter is limited to 20 mas for a better display. The black lines indicate the area used for the sky coverage computation.

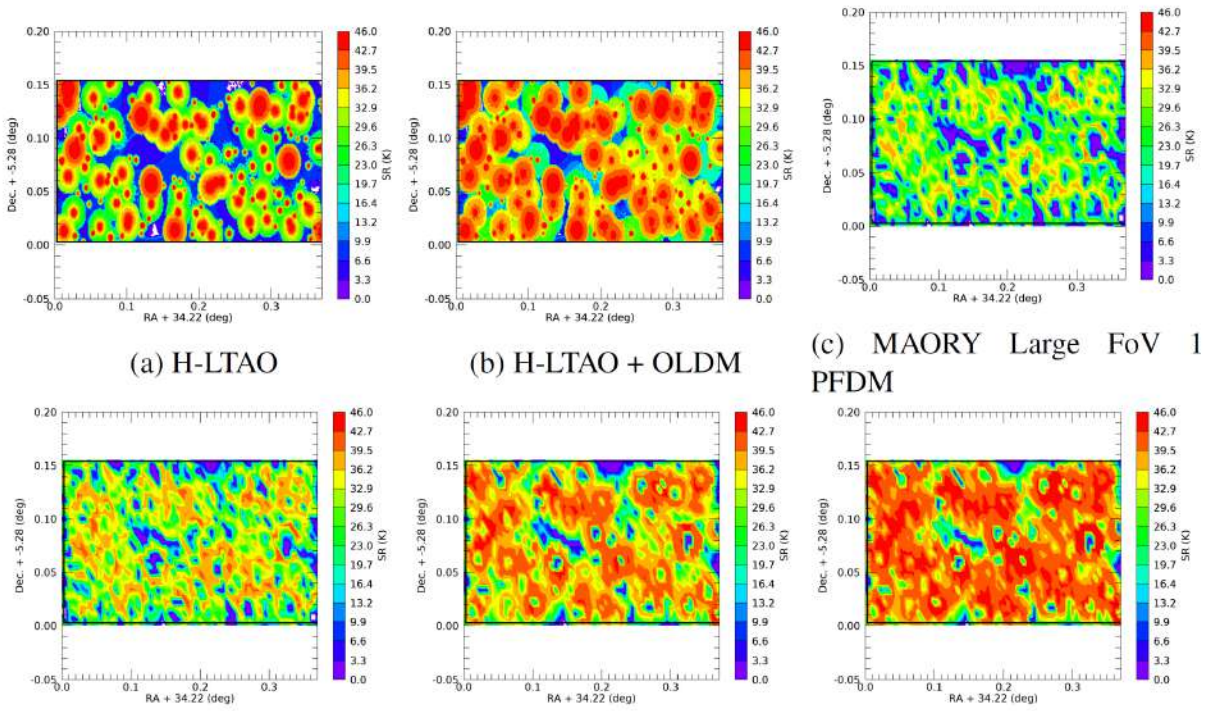

(a) H-LTAO (b) H-LTAO + OLDM (c) MAORY Large FoV 1 PFDM

(d) MAORY Large FoV 2 PFDMs (e) MAORY Small FoV 1 PFDM (f) MAORY Small FoV 2 PFDMs

Figure 16: Strehl ratio in K band with H-LTAO (on axis) or with MAORY (averaged on the scientific FoV) for the UDS field. The black lines indicate the area used for the sky coverage computation.

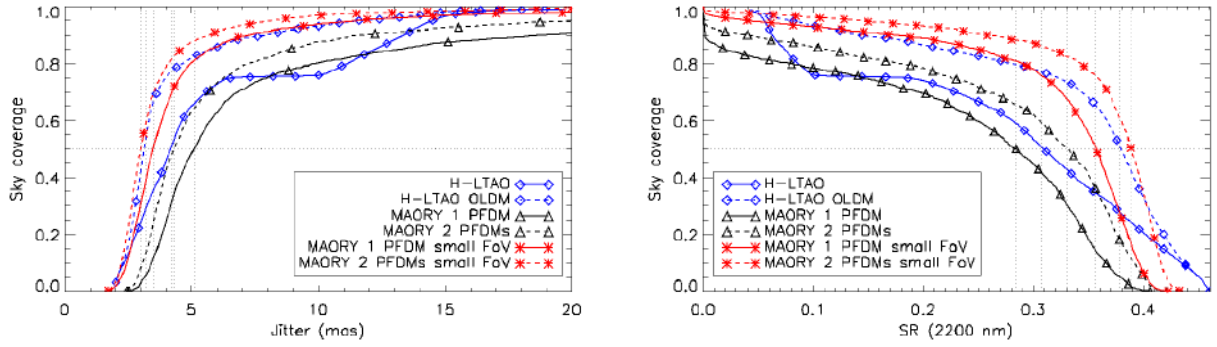

(a) Jitter (b) SR

Figure 17: Sky coverage with H-LTAO or with MAORY for the UDS field. The jitter/SR is on axis for H-LTAO and averaged on a 1 arcmin diameter FoV (Large FoV) or on a 20" diameter FoV (small FoV) for MAORY.

Instrument/configuration	Jitter (mas)			SR (2200 nm)		
	25% SC	50% SC	75% SC	25% SC	50% SC	75% SC
H-LTAO	3.1	4.2	6.5	0.39	0.31	0.19
H-LTAO OLDM	2.7	3.2	4	0.41	0.38	0.32
MAORY 1 PFDM	4	5.1	8	0.34	0.28	0.14
MAORY 2 PFDMs	3.5	4.3	6.3	0.37	0.33	0.23
MAORY 1 PFDM small FoV	2.9	3.5	4.5	0.40	0.38	0.32
MAORY 2 PFDMs small FoV	2.6	3	3.8	0.42	0.40	0.37

Table 7: Jitter/SR reached by the considered systems for different levels of sky coverage in the UDS field.

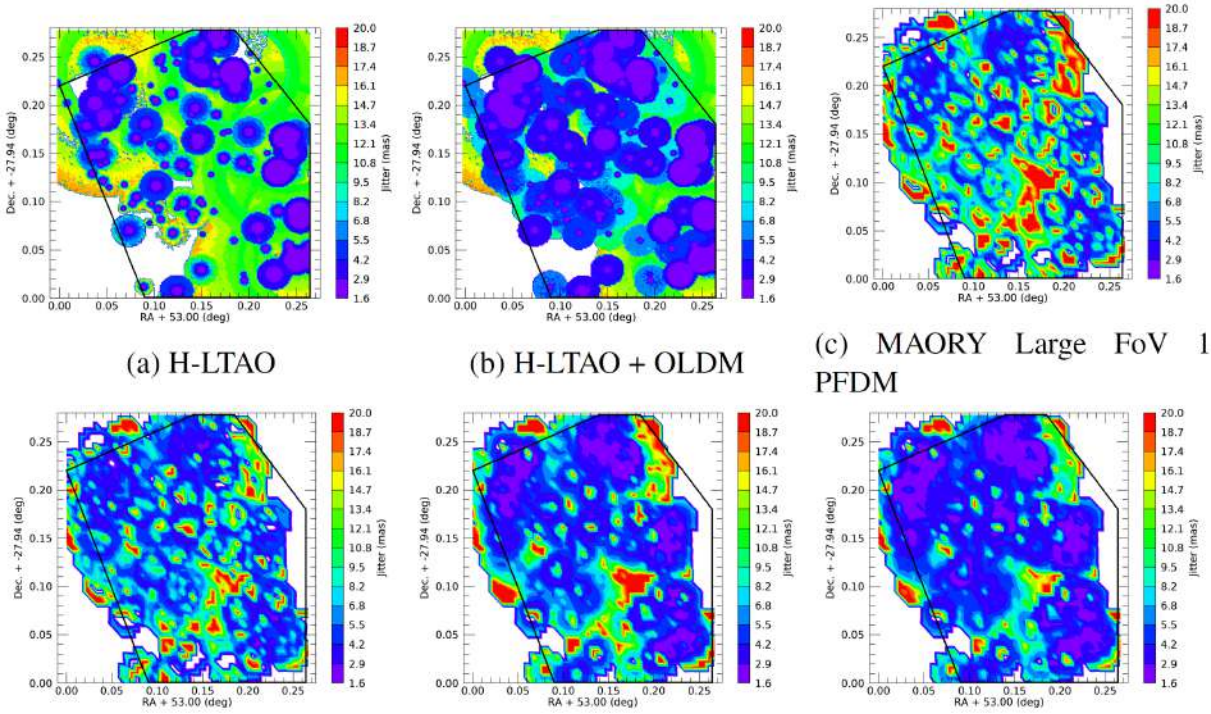

(a) H-LTAO (b) H-LTAO + OLDM (c) MAORY Large FoV 1 PFDM

(d) MAORY Large FoV 2 PFDMs (e) MAORY Small FoV 1 PFDM (f) MAORY Small FoV 2 PFDMs

Figure 18: Jitter with H-LTAO (on axis) or with MAORY (averaged on the scientific FoV) for the GOODS-S field. The jitter is limited to 20 mas for a better display. The black lines indicate the area used for the sky coverage computation.

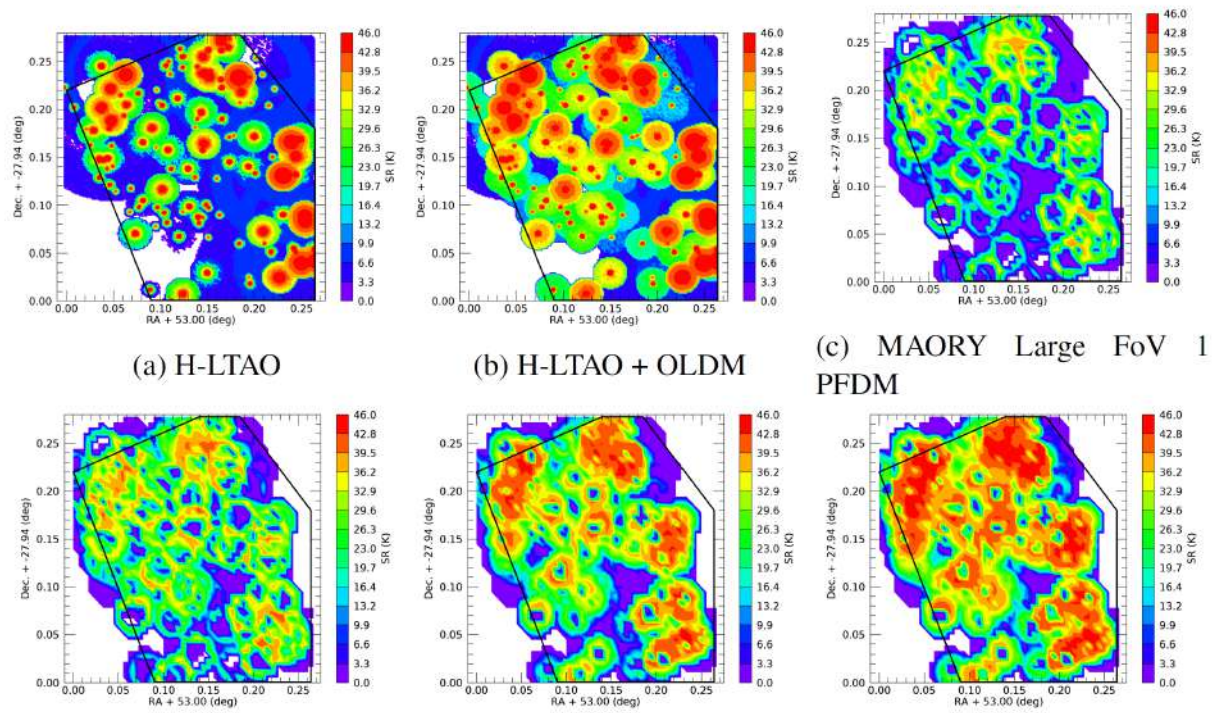

(a) H-LTAO (b) H-LTAO + OLDM (c) MAORY Large FoV 1 PFDM

(d) MAORY Large FoV 2 PFDMs (e) MAORY Small FoV 1 PFDM (f) MAORY Small FoV 2 PFDMs

Figure 19: Strehl ratio in K band with H-LTAO (on axis) or with MAORY (averaged on the scientific FoV) for the GOODS-S field. The black lines indicate the area used for the sky coverage computation.

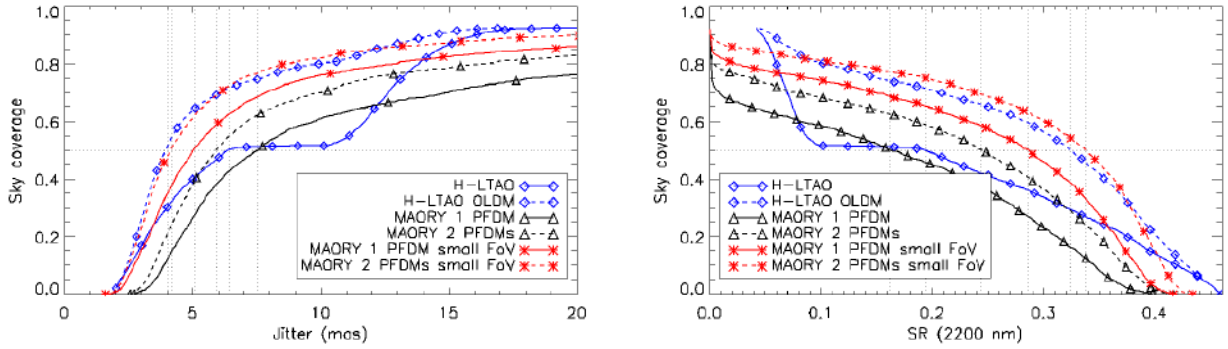

(a) Jitter (b) SR

Figure 20: Sky coverage with H-LTAO or with MAORY for the GOODS-S field. The jitter/SR is on axis for H-LTAO and averaged on a 1 arcmin diameter FoV (Large FoV) or on a 20" diameter FoV (small FoV) for MAORY.

Instrument/configuration	Jitter (mas)			SR (2200 nm)		
	25% SC	50% SC	75% SC	25% SC	50% SC	75% SC
H-LTAO	3.6	6.4	13.2	0.35	0.19	0.06
H-LTAO OLDM	3	4	7.7	0.39	0.32	0.15
MAORY 1 PFDM	4.9	7.5	18.1	0.29	0.16	0
MAORY 2 PFDMs	4.2	5.9	11.8	0.33	0.24	0.04
MAORY 1 PFDM small FoV	3.6	5.1	9.4	0.37	0.30	0.09
MAORY 2 PFDMs small FoV	3.1	4.2	6.9	0.40	0.35	0.20

Table 8: Jitter/SR reached by the considered systems for different levels of sky coverage in the GOODS-S field.

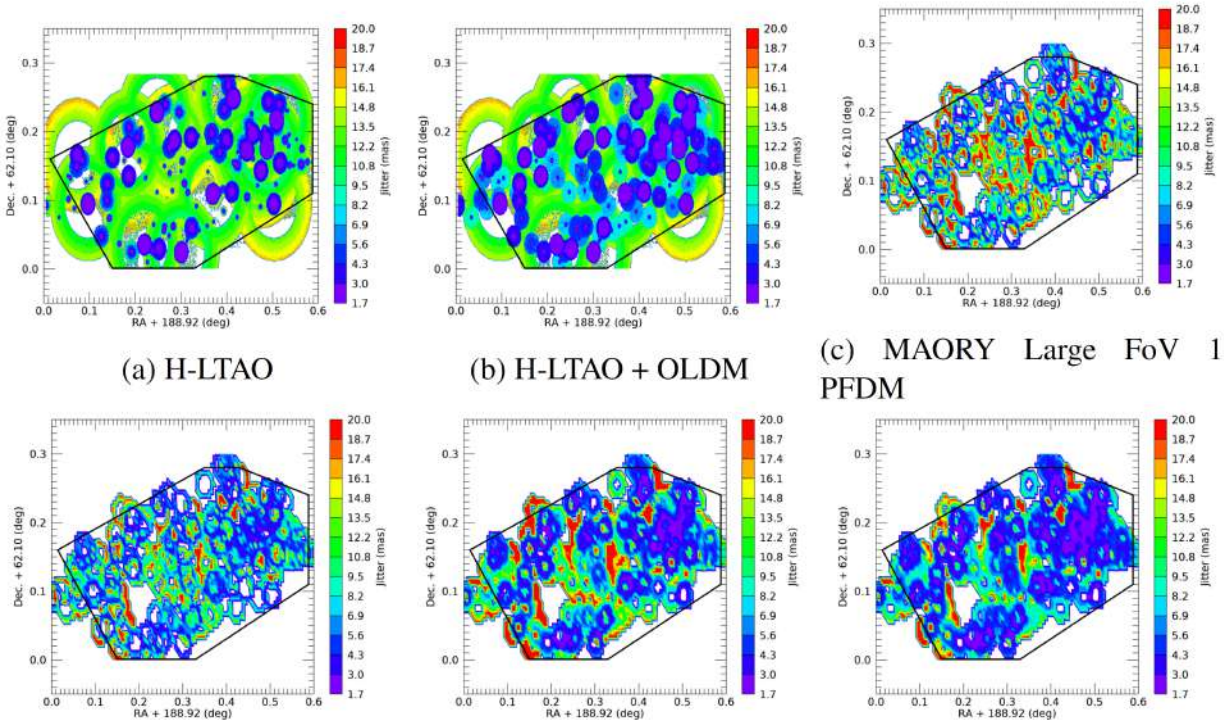

(a) H-LTAO (b) H-LTAO + OLDM (c) MAORY Large FoV 1 PFDM

(d) MAORY Large FoV 2 PFDMs (e) MAORY Small FoV 1 PFDM (f) MAORY Small FoV 2 PFDMs

Figure 21: Jitter with H-LTAO (on axis) or with MAORY (averaged on the scientific FoV) for the GOODS-N field. The jitter is limited to 20 mas for a better display. The black lines indicate the area used for the sky coverage computation.

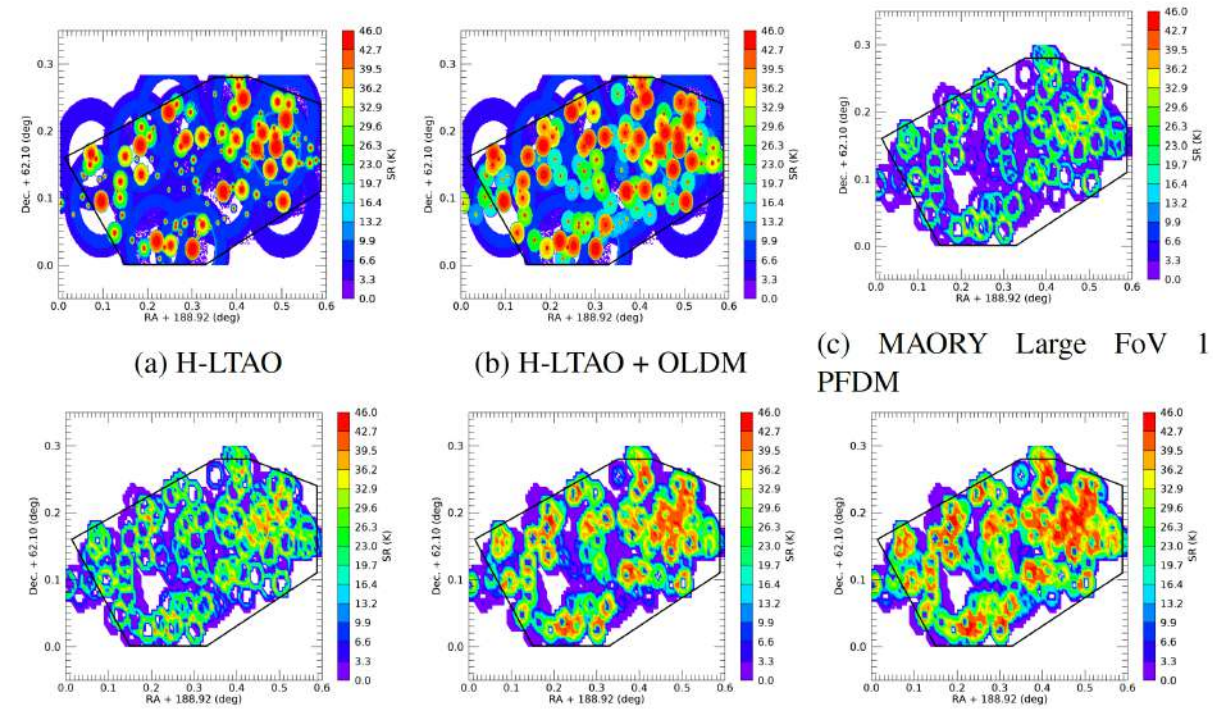

(a) H-LTAO (b) H-LTAO + OLDM (c) MAORY Large FoV 1 PFDM

(d) MAORY Large FoV 2 PFDMs (e) MAORY Small FoV 1 PFDM (f) MAORY Small FoV 2 PFDMs

Figure 22: Strehl ratio in K band with H-LTAO (on axis) or with MAORY (averaged on the scientific FoV) for the GOODS-N field. The black lines indicate the area used for the sky coverage computation.

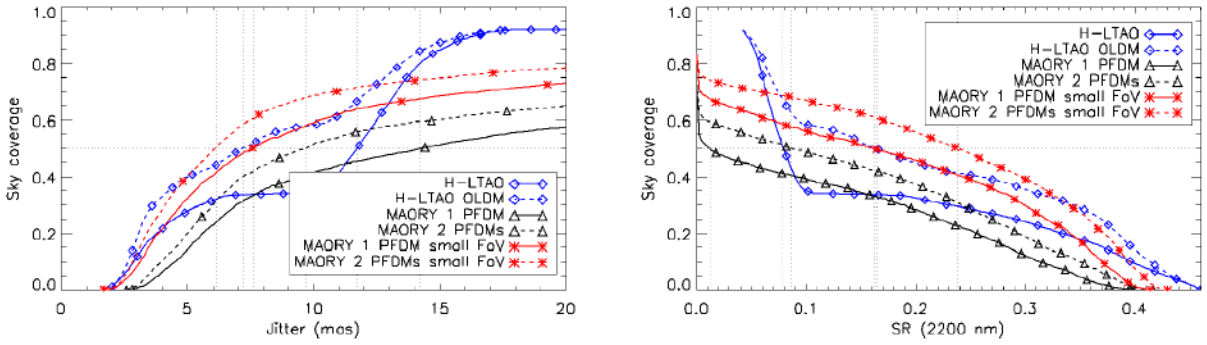

(a) Jitter (b) SR

Figure 23: Sky coverage with H-LTAO or with MAORY for the GOODS-N field. The jitter/SR is on axis for H-LTAO and averaged on a 1 arcmin diameter FoV (Large FoV) or on a 20" diameter FoV (small FoV) for MAORY.

Instrument/configuration	Jitter (mas)			SR (2200 nm)		
	25% SC	50% SC	75% SC	25% SC	50% SC	75% SC
H-LTAO	4.5	11.7	13.7	0.29	0.08	0.06
H-LTAO OLDM	3.3	7.2	12.8	0.37	0.16	0.07
MAORY 1 PFDM	6.3	14.2	119	0.22	0.01	0
MAORY 2 PFDMs	5.5	9.7	63	0.27	0.09	0
MAORY 1 PFDM small FoV	4.3	7.6	23.1	0.34	0.17	0
MAORY 2 PFDMs small FoV	3.8	6.1	15.1	0.37	0.24	0.01

Table 9: Jitter/SR reached by the considered systems for different levels of sky coverage in the GOODS-N field.

5 Discussion

The jitter and SR maps present a recurrent pattern: the performance of MAORY is best around the areas where the performance of H-LTAO is best. Indeed, H-LTAO needs only one NGS, that can be close to the optical axis of the telescope, whereas MAORY makes use of up to 3 NGSs, that need to be at a minimum distance of 49" (large MICADO FoV) or 24" (small MICADO FoV) to avoid vignetting the scientific FoV. This means that the SR delivered by H-LTAO peaks for pointings close to a bright star and drops quickly when going away from this star, while the SR delivered by MAORY reaches a maximum when the NGSs are not within the science FoV. Besides, we note that the two systems reach similar levels of jitter and SR on the bright end. They are thus complementary in terms of SC, meaning that the overall SC of ESO's ELT is extremely good for applications that are common to the two systems.

The H-LTAO performance (without OLDM) shows a sort of bimodal distribution, with a first plateau of performance up to a jitter limit around 10 mas, and then a second increase of SC. This behaviour is explained by the transition between the sequential and cascade mode, where in the first case we use the closest and brightest stars to perform most of the jitter control, while in the second case the telescope guide probe is mostly controlling the jitter. The transition between these

two regimes will highly depend on the telescope guiding performance, and could potentially be optimized. Note that if NGSs fainter than H=19 were considered, the plateau would appear at better performance. On the other hand, the gain brought by the OLDM can also improve the performance in this exact regime, by providing a better residual jitter for far and faint NGS. This translates into a better SR over a wider area of these cosmological field. Is it however important to mention that the OLDM performance gain presented in this study must be seen as the optimistic upper limit. Indeed, the OLDM off-axis performance has been evaluated in an ideal case where only fitting and off-axis tomography were considered in the error budget. Taking into account a more realistic error budget for the OLDM off-axis performance, including for instance the Open Loop control, DM creep, calibration issues etc... would reduce the expected off-axis Strehl, degrade the expected noise propagation, and eventually increase the residual jitter. The final and realistic performance to be expected with OLDM certainly lies in between the two performance plots shown in this study.

For MAORY, the second PFDM also improves the overall SC, but the most significant gain in performance is when considering the small MICADO FoV instead of the large one: it surpasses by far the gain provided by the third DM. This is mostly thanks to the additional area given to the technical FoV, that allows the selection of more stars in general and especially ones closer to the optical axis, which provide a better tomography. It would thus be preferable for a MCAO system to get rid of the central obscuration of the technical FoV as much as possible, for example by sensing the NGSs at a wavelength not used by the science path. Though this solution might put difficult constraints on the design, it can be straightforwardly applied in a system such as MAVIS (MCAO-Assisted Visible Imager and Spectrograph),[28] which will do science in the visible.

6 CONCLUSION

The sky coverage of an instrument is a key feature for observations: having a good resolution on only a few objects strongly limits the studies that can be performed by the astronomers. It is thus important to make sure that future AO systems, such as MAORY and H-LTAO for ESO's ELT, will provide a satisfying SC.

In this paper, we presented the SC assessment methods of MAORY and HARMONI. Though there are some differences between the two approaches, the general method is the same, and could be applied for any other tomographic AO system: evaluate the high-order part of the wavefront error, which is independent from the NGS asterism, then compute the statistics of the low-order part using a series of randomly generated fields. The low-order residuals are the sum of a purely geometric tomographic error, that only depends on the NGS asterism geometry; the noise propagation through the tomographic reconstruction, that depends on the wavefront sensor sensitivity, the NGSs' magnitudes and the correction level in the technical FoV; and the residual vibrations due to windshake. Other terms of wavefront error, that are independent from either the NGS asterism or the whole AO system itself, can be independently added afterwards.

We have then evaluated the performance of both MAORY and H-LTAO in already known cosmological fields. These results can be taken as an indication of the image quality on MICADO and HARMONI in sky areas that are poor in bright stars, hence where the AO is pushed to its limits. We have confirmed that the use of an OLDM can increase the SC of a LTAO system. Likewise, the addition of a second post-focal DM for MAORY provides a significant gain in performance. We also noted that reducing the central obscuration of the technical FoV of MAORY, which happens when using MICADO's small FoV, leads to a much better performance as well. This encourages

the choice of a NGS sensing wavelength not used by the science for MCAO systems, though it might be difficult in practice. Finally, we have shown that, if applications concur, the SC provided by the two systems can be complementary. The overall SC of the telescope is thus greatly improved.

Appendix A: Computation of tomographic error

The goal of this appendix is to compute the LO residual in a direction α due to the tomographic reconstruction error. We assume that we will perform a split tomography, meaning that the high-order (modes from focus, sensed with the LGSs) and low-order modes (tip/tilt, sensed with the NGSs) will be estimated separately. We can thus assess the tomographic error using the NGSs only. We can write the estimation of the LO modes in the direction α as:

$$\hat{a} = R(s + n) \tag{8}$$

where $\hat{a}$ is the estimate of a, the vector of LO modes coefficients in the direction α; s is the vector grouping all the measured LO modes coefficients for all NGSs; n is the noise on these measurements and R is the reconstructor. We define here the reconstructor as:

$$R = P_\alpha W \tag{9}$$

with P_α the projection in the direction α and W the tomographic reconstructor, computed with 2 layers (tip/tilt on ground layer and focus/astigmatism on altitude layer). The covariance matrix of the LO modes in the direction α can then be expressed as (assuming the noise is not correlated

with a nor s):

$$< (a - \hat{a})(a - \hat{a})^t >= C_{aa} - C_{as}R^t - RC_{as}^t + RC_{ss}R^t + RC_{nn}R^t \tag{10}$$

with $C_{xy} =< xy^t >$ the covariance between x and y. The formula to compute these covariance matrices for Zernike modes is given in Appendix B. In this paper, the noise covariance matrix C_{nn} is considered diagonal, with a uniformly distributed noise on the 2 LO modes (example for a 3-NGS asterism with MAORY):

$$C_{nn} = \begin{bmatrix} \sigma_1^2/2 & 0 & \dots & \dots & \dots & 0 \\ 0 & \sigma_1^2/2 & 0 & \dots & \dots & \vdots \\ \vdots & 0 & \sigma_2^2/2 & 0 & \dots & \vdots \\ \vdots & \dots & 0 & \sigma_2^2/2 & 0 & \vdots \\ \vdots & \dots & \dots & 0 & \sigma_3^2/2 & 0 \\ 0 & \dots & \dots & \dots & 0 & \sigma_3^2/2 \end{bmatrix} \tag{11}$$

with σ_k^2 the total noise variance on the k-th NGS.

We can finally define the tomographic error as:

$$\sigma_{tomo,tot} = \sqrt{\sigma_{tomo,0}^2 + \sigma_{tomo,n}^2} \tag{12}$$

with

$$\sigma_{tomo,0}^2 = C_{aa} - C_{as}R^t - RC_{as}^t + RC_{ss}R^t \tag{13}$$

the pure tomographic error and

$$\sigma^2_{tomo,n} = RC_{nn}R^t \tag{14}$$

the tomographic noise error.

Appendix B: Computation of Zernike modes covariances

The covariance between 2 Zernike mode coefficients a_j and a_k (in Noll's definition[29]) in the direction of 2 different stars at coordinates $\overrightarrow{\theta_1}$ and $\overrightarrow{\theta_2}$ is, for a telescope of radius R:[30]

$$\begin{aligned}
< a_j\left(\overrightarrow{\theta_1}\right) a_k\left(\overrightarrow{\theta_2}\right) > =& (-1)^{m_k}\sqrt{(n_j+1)(n_k+1)}\, i^{n_j+n_k} 2^{1-0.5(\delta_{0m_j}+\delta_{0m_k})} \\
&\times \int dh \frac{1}{\pi R^2\left(1-\frac{h}{z_1}\right)\left(1-\frac{h}{z_2}\right)} \\
&\times \int_0^\infty \frac{df}{f} W_\varphi(h,f) J_{n_j+1}\left(2\pi f R\left(1-\frac{h}{z_1}\right)\right) J_{n_k+1}\left(2\pi f R\left(1-\frac{h}{z_2}\right)\right) \\
&\times \Bigg\{ cos\Big((m_j+m_k) arg\left(\overrightarrow{\theta_1}-\overrightarrow{\theta_2}\right) \\
&+\frac{\pi}{4}\left(\left(1-\delta_{0m_j}\right)\left((-1)^j-1\right)+\left(1-\delta_{0m_k}\right)\left((-1)^k-1\right)\right)\Big) \\
&\times i^{3(m_j+m_k)} J_{m_j+m_k}\left(2\pi f h|\overrightarrow{\theta_1}-\overrightarrow{\theta_2}|\right) \\
&+cos\Big((m_j-m_k) arg\left(\overrightarrow{\theta_1}-\overrightarrow{\theta_2}\right) \\
&+\frac{\pi}{4}\left(\left(1-\delta_{0m_j}\right)\left((-1)^j-1\right)-\left(1-\delta_{0m_k}\right)\left((-1)^k-1\right)\right)\Big) \\
&\times i^{3|m_j-m_k|} J_{|m_j-m_k|}\left(2\pi f h|\overrightarrow{\theta_1}-\overrightarrow{\theta_2}|\right) \Bigg\}
\end{aligned} \tag{15}$$

with n_j and m_j the radial and azimuthal orders of the j-th polynomial, δ_{0x} the Kronecker delta between 0 and x, h the layer altitude, z_1 and z_2 the altitudes of the 2 stars (= infinity for NGSs), $J_n(x)$ the Bessel function of first kind of order n, f the spatial frequency and $W_\varphi(h,f)$ the turbulent

phase PSD for the layer at altitude h. The turbulent PSD used in this paper is the one defined by Von-Karman:

$$W_\varphi(h, f) = 0.023 r_0(h)^{-\frac{5}{3}} \left(f^2 + \frac{1}{L_0^2} \right)^{-\frac{11}{6}} \tag{16}$$

with r_0 the Fried parameter and L_0 the outer scale (= 25 m throughout the paper).

Appendix C: Model validation

For MAORY, the LO residual (without windshake) in one direction of the scientific FoV is computed from the noise error interpolation described in section 3.2.4 and the tomographic error described in section 3.2.3. This residual can be verified with E2E simulations. We performed a sanity check of the residual on axis with the asterisms used for the noise interpolation on one hand (Fig. 24), and random 3-NGS asterisms on the other hand (Fig. 25). The random asterisms have distance and magnitude values chosen from the ones of section 3.2.4 and the angle values are limited to steps of 30°. The pick-up mirror collisions were not considered, so 2 stars could fall at the same place, thus some of the asterisms are equivalent to 2-NGS asterisms.

We have a good match between the real residual and the estimated one. On the equilateral asterisms (Fig. 24), we see that we might overestimate a bit the error at high flux and underestimate it at low flux, but we always fall within the error bars, which we consider a sufficient level of precision for this analysis. Looking at random asterisms (Fig. 25) that represent more significantly what we can expect in the SC analysis, the match is satisfying as well. We thus consider that our model is valid.

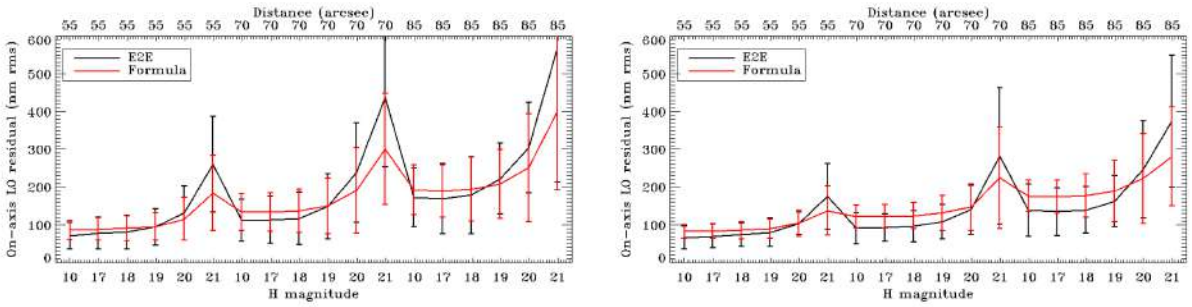

(a) 1 PFDM (b) 2 PFDMs

Figure 24: Comparison of the LO residual on axis from the end-to-end simulations and from the formula. Left: with 1 PFDM. Right: with 2 PFDMs. All asterisms are equilateral triangles, with all the stars at the same distance and the same magnitude (indicated on the x axes).

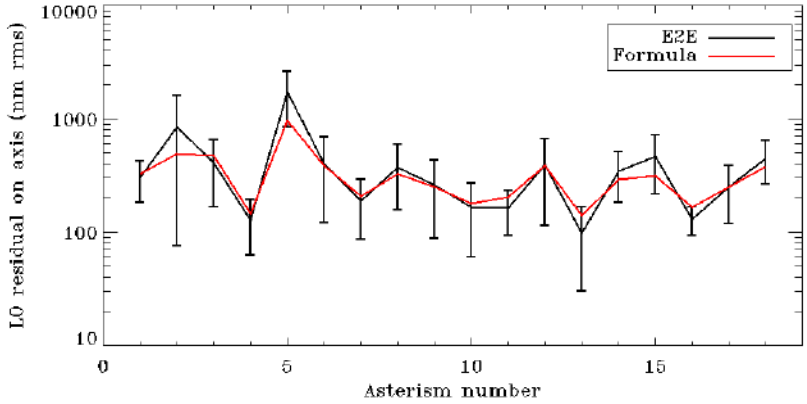

Figure 25: Comparison of the LO residual on axis from the end-to-end simulations and from the formula, for 18 random asterisms and 2 DMs.

In the case of H-LTAO, a comparison between the E2E simulation and the modified analytical model is shown in figure 26.

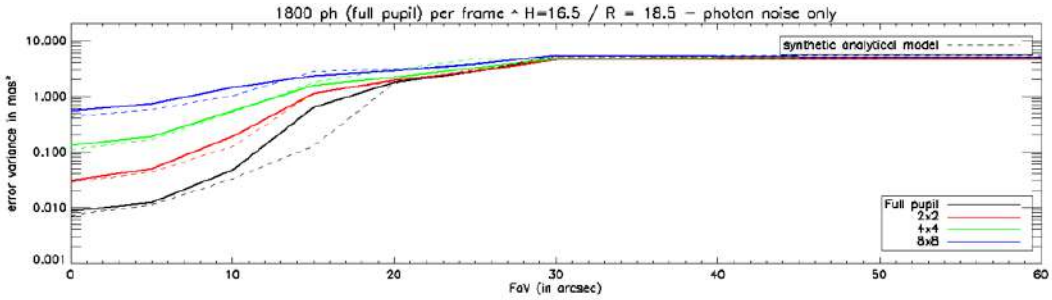

Figure 26: Evolution of the noise variance (in mas^2) as a function of the FoV position. Solid line = Simulation. Dotted line = analytical expression in the good SR regime, Dashed-line = FWHM regime.

Note that we checked that similar good match between the analytical model and the E2E simulations were valid for other fluxes levels. We also checked the good behaviour of the model when RON is added.

Disclosures

The authors declare no conflict of interest.

Acknowledgments

This project received funding from the European Union's Horizon 2020 research and innovation programme under the Marie Sklodowska-Curie grant agreement No 893150. This work also benefited from the support of the WOLF project ANR-18-CE31-0018 of the French National Research Agency (ANR). This document has been prepared as part of the activities of OPTICON H2020 (2017-2020) Work Package 1 (Calibration and test tools for AO assisted E-ELT instruments). OPTICON is supported by the Horizon 2020 Framework Programme of the European Commission's (Grant number 730890). This work was supported by the Action Spécifique Haute Résolution Angulaire (ASHRA) of CNRS/INSU co-funded by CNES. This work has been partially supported by the LabEx FOCUS ANR-11-LABX-0013.

This work was also partially funded by the grant Premiale ADONI Cram 1.05.06.07 chiave MAORY.

References

1 "European Extremely Large Telescope ESO." https://www.eso.org/public/france/teles-instr/elt/. Accessed: 2010-09-30.

2 P. Ciliegi, E. Diolaiti, R. Abicca, *et al.*, "MAORY for ELT: preliminary design overview," in *SPIE Proceedings*, *Society of Photo-Optical Instrumentation Engineers (SPIE) Conference Series* **10703**, 1070311 (2018).

3 R. Davies *et al.*, "MICADO: first-light imager for the E-ELT," *SPIE Proceedings* (2016).

4 N. A. Thatte, F. Clarke, I. Bryson, *et al.*, "The E-ELT first light spectrograph HARMONI: capabilities and modes," in *SPIE Proceedings*, *Society of Photo-Optical Instrumentation Engineers (SPIE) Conference Series* **9908**, 99081X (2016).

5 B. Neichel, T. Fusco, J. F. Sauvage, *et al.*, "The adaptive optics modes for HARMONI: from Classical to Laser Assisted Tomographic AO," in *SPIE Proceedings*, *Society of Photo-Optical Instrumentation Engineers (SPIE) Conference Series* **9909**, 990909 (2016).

6 B. R. Brandl, O. Absil, T. Agócs, *et al.*, "Status of the mid-IR ELT imager and spectrograph (METIS)," in *SPIE Proceedings*, *Society of Photo-Optical Instrumentation Engineers (SPIE) Conference Series* **10702**, 107021U (2018).

7 F. Vidal, M. Rozel, V. Deo, *et al.*, "Analysis the MICADO-MAORY SCAO performance," in *Proceedings of the AO4ELT6 conference*, 251 (2019).

8 N. Schwartz, J.-F. Sauvage, E. Renault, *et al.*, "Design of the HARMONI Pyramid WFS module," *arXiv e-prints* , arXiv:2003.07228 (2020).

9 T. Bertram, O. Absil, P. Bizenberger, *et al.*, "Single conjugate adaptive optics for METIS," in *SPIE Proceedings*, *Society of Photo-Optical Instrumentation Engineers (SPIE) Conference Series* **10703**, 1070314 (2018).

10 B. L. Ellerbroek and D. W. Tyler, "Adaptive Optics Sky Coverage Calculations for the

Gemini-North Telescope," *Publications of the Astronomical Society of the Pacific* **110**, 165–185 (1998).

11 M. Le Louarn, R. Clare, C. Béchet, *et al.*, "Simulations of adaptive optics systems for the E-ELT," in *SPIE Proceedings*, *Society of Photo-Optical Instrumentation Engineers (SPIE) Conference Series* **8447**, 84475D (2012).

12 M. Tallon and R. Foy, "Adaptive telescope with laser probe: isoplanatism and cone effect.," *Astronomy and Astrophysics* **235**, 549–557 (1990).

13 B. L. Ellerbroek and F. Rigaut, "Methods for correcting tilt anisoplanatism in laser-guide-star-based multiconjugate adaptive optics," *Journal of the Optical Society of America A* **18**, 2539–2547 (2001).

14 T. Fusco, J.-M. Conan, G. Rousset, *et al.*, "Optimal wave-front reconstruction strategies for multiconjugate adaptive optics," *Journal of the Optical Society of America A* **18**, 2527–2538 (2001).

15 R. Foy and A. Labeyrie, "Feasibility of adaptive telescope with laser probe," *Astronomy and Astrophysics* **152**, L29–L31 (1985).

16 T. Fusco, A. Blanc, M. Nicolle, *et al.*, "Sky coverage estimation for multiconjugate adaptive optics systems: strategies and results," *Monthly Notice of the National Royal Astronomy Society* **370**, 174–184 (2006).

17 D. Andersen, L. Wang, B. Ellerbroek, *et al.*, "Predicted sky coverage for the TMT MCAO system NFIRAOS," in *Second International Conference on Adaptive Optics for Extremely Large Telescopes. Online at ¡A href=“http://ao4elt2.lesia.obspm.fr”¿http://ao4elt2.lesia.obspm.fr¡/A*, P18 (2011).

18 I. Damjanov, R. G. Abraham, K. Glazebrook, *et al.*, "Extragalactic Fields Optimized for Adaptive Optics," *Publications of the Astronomical Society of the Pacific* **123**, 348 (2011).

19 A. Robin and M. Creze, "Stellar populations in the milky way: a synthetic model.," *Astronomy and Astrophysics* **157**, 71–90 (1986).

20 N. A. Grogin, D. D. Kocevski, S. M. Faber, *et al.*, "CANDELS: THE COSMIC ASSEMBLY NEAR-INFRARED DEEP EXTRAGALACTIC LEGACY SURVEY," *The Astrophysical Journal Supplement Series* **197**, 35 (2011).

21 A. M. Koekemoer, S. M. Faber, H. C. Ferguson, *et al.*, "CANDELS: THE COSMIC ASSEMBLY NEAR-INFRARED DEEP EXTRAGALACTIC LEGACY SURVEY—THE HUBBLE SPACE TELESCOPE OBSERVATIONS, IMAGING DATA PRODUCTS, AND MOSAICS," *The Astrophysical Journal Supplement Series* **197**, 36 (2011).

22 J. Kolb, E. Marchetti, D. Schneller, *et al.*, *Relevant Atmospheric Parameters for E-ELT AO Analysis and Simulations* (2015). Internal document ESO-258292, version 2.

23 T. Fusco, J.-M. Conan, G. Rousset, *et al.*, "Optimal wave-front reconstruction strategies for multiconjugate adaptive optics," *J. Opt. Soc. Am. A* **18**, 2527–2538 (2001).

24 T. Pfrommer and P. Hickson, "High-resolution lidar observations of mesospheric sodium and implications for adaptive optics," *Journal of the Optical Society of America A* **27**, A97 (2010).

25 F. Rigaut and E. Gendron, "Laser guide star in adaptive optics: the tilt determination problem.," *Astronomy and Astrophysics* **261**, 677–684 (1992).

26 "Data package for ELT simulations." ESO-315732.

27 M. Nicolle, T. Fusco, G. Rousset, *et al.*, "Improvement of shack–hartmann wave-front sensor measurement for extreme adaptive optics," *Optics Letters* **29**(23), 2743–2745 (2004).

529 28 F. Rigaut, R. McDermid, G. Cresci, *et al.*, "MAVIS conceptual design," in *Ground-based and*
530 *Airborne Instrumentation for Astronomy VIII*, C. J. Evans, J. J. Bryant, and K. Motohara,
531 Eds., **11447**, 378 – 393, International Society for Optics and Photonics, SPIE (2020).
532 29 R. J. Noll, "Zernike polynomials and atmospheric turbulence," *Opt. Soc. Am.* **66** (1976).
533 30 M. R. Whiteley, M. C. Roggemann, and B. M. Welsh, "Temporal properties of the Zernike
534 expansion coefficients of turbulence-induced phase aberrations for aperture and source mo-
535 tion," *J. Opt. Soc. Am. A* **15**, 993–1005 (1998).

536 **Cédric Plantet** got his PhD in 2014, from the Paris Observatory University. His work was fo-
537 cused on focal-plane wavefront sensing with the LIneraized Focal-plane Technique (LIFT). After
538 a first post-doc at Onera and LAM on infrared wavefront sensing, he joined INAF - Osservatorio
539 Astrofisico di Arcetri in 2016 to work on MAORY and then other Adaptive Optics projects such
540 as MAVIS. His current work is mostly focused on semi-analytical simulations for Adaptive Optics
541 and natural guide star wavefront sensing.

542 **Benoît Neichel** got his PhD in 2008, from the Paris Observatory University. His work was focused
543 on Integral Field Spectroscopy (IFS) observations of distant galaxies, and on Wide Field Adaptive
544 Optics (WFAO) systems for extragalactic observations on Extremely Large Telescopes (ELTs). He
545 then worked as Instrument Scientist for the Gemini GeMS instrument, which was the first WFAO
546 system implemented on an 8m telescope and offered to the astronomical community. In 2013 he
547 joined LAM - Laboratoire d'Astrophysique de Marseille - as full time scientist. He is now the
548 deputy-PI for HARMONI the first light IFS for the European ELT, and he is leading the Research
549 & Development department of LAM.

Biographies and photographs of the other authors are not available.

List of Figures

4 Example of noise computed for a 2x2 SHWFS, for different level of fluxes, and different position of the NGS in the field, in the case of an LTAO correction without OLDM.

5 Directions used for the jitter/SR computation in the FoV of diameter 60". The square of side 53" corresponds to the large MICADO FoV. The stars are distributed as follows: 1 star on axis, 4 stars at 15", 4 stars at 25" and 4 stars at 30". When the small MICADO FoV is considered (20×20"), we average from 1 star on axis and 4 stars at 10" (placed in the same manner as the 4 stars at 15").

6 Sky coverage with H-LTAO or with MAORY at $l = 90°, b = -30°$. The jitter/SR is on axis for H-LTAO and averaged on a 1 arcmin diameter FoV (Large FoV) or on a 20" diameter FoV (small FoV) for MAORY.

7 Sky coverage with H-LTAO or with MAORY at $l = 90°, b = -60°$. The jitter/SR is on axis for H-LTAO and averaged on a 1 arcmin diameter FoV (Large FoV) or on a 20" diameter FoV (small FoV) for MAORY.

8 Cosmological fields considered in this section. Taken from Grogin et al.[20].

9 Jitter with H-LTAO (on axis) or with MAORY (averaged on the scientific FoV) for the COSMOS field. The jitter is limited to 20 mas for a better display. The black lines indicate the area used for the sky coverage computation.

10 Strehl ratio in K band with H-LTAO (on axis) or with MAORY (averaged on the scientific FoV) for the COSMOS field. The black lines indicate the area used for the sky coverage computation.

11 Sky coverage with H-LTAO or with MAORY for the COSMOS field. The jitter/SR is on axis for H-LTAO and averaged on a 1 arcmin diameter FoV (Large FoV) or on a 20” diameter FoV (small FoV) for MAORY.

12 Jitter with H-LTAO (on axis) or with MAORY (averaged on the scientific FoV) for the EGS field. The jitter is limited to 20 mas for a better display. The black lines indicate the area used for the sky coverage computation.

13 Strehl ratio in K band with H-LTAO (on axis) or with MAORY (averaged on the scientific FoV) for the EGS field. The black lines indicate the area used for the sky coverage computation.

14 Sky coverage with H-LTAO or with MAORY for the EGS field. The jitter/SR is on axis for H-LTAO and averaged on a 1 arcmin diameter FoV (Large FoV) or on a 20” diameter FoV (small FoV) for MAORY.

15 Jitter with H-LTAO (on axis) or with MAORY (averaged on the scientific FoV) for the UDS field. The jitter is limited to 20 mas for a better display. The black lines indicate the area used for the sky coverage computation.

16 Strehl ratio in K band with H-LTAO (on axis) or with MAORY (averaged on the scientific FoV) for the UDS field. The black lines indicate the area used for the sky coverage computation.

17 Sky coverage with H-LTAO or with MAORY for the UDS field. The jitter/SR is on axis for H-LTAO and averaged on a 1 arcmin diameter FoV (Large FoV) or on a 20” diameter FoV (small FoV) for MAORY.

18 Jitter with H-LTAO (on axis) or with MAORY (averaged on the scientific FoV) for the GOODS-S field. The jitter is limited to 20 mas for a better display. The black lines indicate the area used for the sky coverage computation.

19 Strehl ratio in K band with H-LTAO (on axis) or with MAORY (averaged on the scientific FoV) for the GOODS-S field. The black lines indicate the area used for the sky coverage computation.

20 Sky coverage with H-LTAO or with MAORY for the GOODS-S field. The jitter/SR is on axis for H-LTAO and averaged on a 1 arcmin diameter FoV (Large FoV) or on a 20" diameter FoV (small FoV) for MAORY.

21 Jitter with H-LTAO (on axis) or with MAORY (averaged on the scientific FoV) for the GOODS-N field. The jitter is limited to 20 mas for a better display. The black lines indicate the area used for the sky coverage computation.

22 Strehl ratio in K band with H-LTAO (on axis) or with MAORY (averaged on the scientific FoV) for the GOODS-N field. The black lines indicate the area used for the sky coverage computation.

23 Sky coverage with H-LTAO or with MAORY for the GOODS-N field. The jitter/SR is on axis for H-LTAO and averaged on a 1 arcmin diameter FoV (Large FoV) or on a 20" diameter FoV (small FoV) for MAORY.

24 Comparison of the LO residual on axis from the end-to-end simulations and from the formula. Left: with 1 PFDM. Right: with 2 PFDMs. All asterisms are equilateral triangles, with all the stars at the same distance and the same magnitude (indicated on the x axes).

List of Tables

7 Jitter/SR reached by the considered systems for different levels of sky coverage in the UDS field.

8 Jitter/SR reached by the considered systems for different levels of sky coverage in the GOODS-S field.

9 Jitter/SR reached by the considered systems for different levels of sky coverage in the GOODS-N field.